Bioresource Technology Reports 31 (2025) 102208

Contents lists available at ScienceDirect

Bioresource Technology Reports

journal homepage: www.sciencedirect.com/journal/bioresource-technology-reports

Impact of the rotational speed and counter electrode configuration on the performance of a rotating disc bioelectrochemical reactor (RDBER) operated as microbial electrolysis cell☆

Zhizhao Xiao [a], Max Rümenapf [a], Max Hackbarth [a], Andrea Hille-Reichel [a], Harald Horn [a,b], Johannes Eberhard Reiner [a,*,1]

[a] Engler-Bunte-Institut, Water Chemistry and Water Technology, Karlsruhe Institute of Technology (KIT), Engler-Bunte-Ring 9a, 76131 Karlsruhe, Germany
[b] DVGW Research Centre, Water Chemistry and Water Technology, Engler-Bunte-Ring 9a, 76131 Karlsruhe, Germany

ARTICLE INFO

Keywords:
Single-chamber microbial electrolysis cell
Bench-scale
Hydrogen production
Hydrogen-shuttling mitigation
Rotating electrodes
Shewanella oneidensis
Geobacter sulfurreducens

ABSTRACT

A 10 L Rotating Disc Bioelectrochemical Reactor (RDBER) was operated as a microbial electrolysis cell (MEC) under different rotational speeds and counter electrode configurations. Increasing the anode's speed from 0.25 to 1 rpm raised the anodic current density from 0.55 ± 0.14 to 1.00 ± 0.07 A m^{-2} while increasing hydrogen production rates from 0.05 ± 0.01 to 0.18 ± 0.01 L_{H_2} L_R^{-1} d^{-1}. Higher speeds provided no further benefit. Moving the counter electrodes to the upper reactor half reduced observed hydrogen shuttling. The modified RDBER reached current densities of 1.98 ± 0.11 A m^{-2} and 0.99 ± 0.03 L_{H_2} L_R^{-1} d^{-1} hydrogen production. Optical coherence tomography confirmed biofilm morphology changes but no significant increase in biovolume or substratum coverage. Hydrogen recovery remained below 50 %. While the RDBER achieved high volumetric current densities and volumetric hydrogen production rates compared to other MEC pilots, improvements in anodic current density and cathodic hydrogen recovery are required for practical application.

1. Introduction

Microbial electrochemical technologies (METs) intertwine applied electrochemistry with microbial metabolism, either directly or indirectly (Schröder et al., 2015). METs are receiving research attention mainly due to their potential contribution to electricity-driven waste stream transformations within a future sustainable economy (Ieropoulos et al., 2024; Jiang et al., 2023; Jourdin and Burdyny, 2021). A specific implementation of this technology is a microbial electrolysis cell (MEC). Here, the exergonic microbial degradation of organic compounds is electrically linked to an abiotic, cathodic hydrogen production (Rozendal et al., 2006). Since the anode reaction is driven by the microbial oxidation of organic substrates (e.g. acetate/CO_2, $E^{\circ\prime} \approx -0.29$) instead of water oxidation (H_2O/O_2, $E^{\circ\prime} \approx 0.82$ V), the electrical energy input required to drive the cathodic hydrogen evolution reaction (H^+/H_2, $E^{\circ\prime} \approx -0.41$) can be significantly lower in a MEC compared to conventional water electrolysis (Kim et al., 2025). In this way, MECs have positioned themselves at the forefront of the evolving field of METs - by coupling the treatment of carbon-rich waste streams with the surplus of an electrocatalytic hydrogen production. Microbial electrochemical technologies have undergone extensive laboratory study over the last decades and are currently finding their way into pilot-scale implementations (Das and Ghangrekar, 2024). Inevitably, this also drives the development of novel reactor designs to meet the scaled demands of a pilot plant (Enzmann et al., 2019). For a more detailed overview of MEC fundamentals and recent advances, readers are referred to comprehensive reviews on this topic (Jiang et al., 2023; Rousseau et al., 2020).

MECs are typically classified into dual-chamber and single-chamber reactors, depending on whether the anode and cathode compartments are physically separated by a selectively permeable membrane. At the laboratory scale (<1 L reactor volume), zero-gap flow cells clearly outperform other reactor concepts in the pursuit of increased current densities and enhanced hydrogen production rates (Kim et al., 2025). These zero-gap designs are optimized versions of a conventional dual-chamber MEC reactor, that employs a membrane separating anode and cathode chambers to ensure hydrogen purity and prevent

☆ Max Hackbarth deceased on November 19, 2024 - prior to the submission of this article.

* Corresponding author.
E-mail address: jer@corc.au.dk (J.E. Reiner).
[1] Present address: The Novo Nordisk Foundation CO_2 Research Center (CORC), Aarhus University, Gustav Wieds Vej 10C, 8000 Aarhus, Denmark.

https://doi.org/10.1016/j.biteb.2025.102208
Received 11 March 2025; Received in revised form 30 June 2025; Accepted 2 July 2025
Available online 8 July 2025

electrochemical short circuits (Gautam et al., 2023). However, while the ongoing development of zero-gap flow cells partly addressed challenges associated with conventional membrane-based MEC designs – such as the formation of pH gradients and increased internal resistances (Bian et al., 2024; Rossi et al., 2023, 2022) – high operational costs related to maintenance and membrane fouling might remain a significant issue (Kracke et al., 2018). Noteworthy, the outstanding performance of these systems is currently limited to rather small-scale reactors (a few milliliters in anodic working volume), which appear to be at least challenging to scale linearly. Hence, it is often proposed that the increase in reactor working volume and electrode surface area should be achieved through numbering up of small dual-chamber zero-gap reactors (Enzmann et al., 2019). The modular design of commercial-scale water electrolyzers is often held up as a reference, as a similar stacking concept is already practiced here. Yet, connecting thousands of individual modules in order to provide sufficient anode working volume required to treat real liquid waste streams may result in a plethora of potential leakage points which considerably complicates periodic inspection and maintenance during long-term operation. Besides, prolonged narrow flow channels could also lead to high flow resistances leading to pressure drops that might result in uneconomical pumping energy demands. Additionally, the narrow flow channels of current zero gap designs may be prone to clogging due to biofilm formation and/or suspended solids in real waste streams (Kim et al., 2025). Finally, the distribution of inter-cell voltages in large stacks remains unknown, as do possible pH and nutrient gradients that may develop within or between individual stacks.

Taken together, while clearly demonstrating the most promising performance on a small scale, numbered-up dual-chamber MECs may not (yet) be suitable for all large-scale MET applications, such as treating high volumetric waste streams with an elevated content of suspended solids. Hence, novel creative reactor concepts that circumvent these limitations of conventional MEC-architectures could facilitate a broader implementation of METs beyond the laboratory, enabling practical deployment in large-scale waste treatment and bioelectrochemical production.

Along these lines, a novel reactor design - the Rotating Disc Bioelectrochemical Reactor (RDBER) - has recently been introduced (Hackbarth et al., 2023). The RDBER employs 14 rotating graphite discs as working electrodes, providing a total working electrode surface area of 1 m^2 within a 10 L reactor volume, thereby offering a convenient ratio of working electrode surface area to reactor volume of 100:1. Conceptually, the RDBER design allows for easy scaling while maintaining the surface-to-volume ratio for example by elongating the reactor chamber, thereby increasing the number of graphite discs that can be mounted on the rotating shaft (Pott, 2023). The reactor is fully autoclavable, can be chemically sterilized in situ and is thus, in combination with the integrated temperature control, especially suitable for axenic cultivations a prerequisite for many biotech applications. As a single-chamber bioelectrochemical system (BES), the RDBER deliberately avoids the use of membranes. While simplifying the reactor design and avoiding complications caused by membrane fouling and membrane failure on the one hand, such a single-chamber system can be prone to electrochemical short circuits, that can result in decreased efficiencies compared to a conventional two-chamber set up. Hydrogen shuttling is a commonly reported example for such an electrochemical short-circuit of a single-chamber MEC (Knoll et al., 2023). Here, the cathodically produced hydrogen gets reoxidized into protons by the electroactive, anodic biofilm. This short circuit decouples the current densities in the MEC from the net hydrogen production of a MEC. As a result, the electrical energy supplied to the MEC no longer correlates directly with the amount of hydrogen produced. Whether this significant disadvantage of a single-chamber MEC can be offset by the advantages of reduced costs and complexity in reactor design will be shown in future studies on an optimized pilot scale and long-term continuous operation under real conditions.

Although similar in name, the rotating disc bioelectrochemical reactor (RDBER) presented in this study is not derived from the rotating disc electrode (RDE) technique used in analytical electrochemistry. While RDEs typically operate at several hundred to thousands of revolutions per minute (rpm) to study mass transport under well-defined conditions, the RDBER is based on the design principles of rotating biological contactors (RBCs), commonly used in wastewater treatment (Hassard et al., 2015). RBCs consist of closely spaced discs that serve as biofilm substratum, mounted on a rotatable horizontal shaft. Here, the rotation of the half-submerged discs through the bulk medium and the oxic gas phase of the reactor ensures the supply of gaseous and dissolved substrate and nutrients to the biofilm, thereby reducing the reliance on energy-intensive pumping or stirring to aerate the bulk phase. RBCs are characterized by low maintenance and operating costs, ease of process control, and a compact design (high surface area to volume ratio) (Cortez et al., 2008). Initial efforts to integrate bioelectrochemical functionality into RBCs have already been successfully demonstrated at the laboratory scale. Table 1 summarizes studies and their respective objectives presenting BES that incorporate design features inspired to varying extents by RBCs. Notably, apart from the advanced BES incorporating polarity inversion presented by Cheng et al., the RDBER is the only RBC-like reactor in which anodic biofilms have been cultivated on the rotating discs. In all other designs, the anodes remain stationary while the rotating cathodes facilitate either abiotic or biologically mediated reduction reactions (Cheng et al., 2011).

In an RBC a faster rotation of the discs not only counteracts the limiting diffusive transfer of nutrients and (gaseous) substrates into the biofilm, it also directly increases the shear force acting on the biofilm and influences the overall energy consumption of the system. Therefore, the rotational speed of the substratum can be defined as a key operating parameter of an RBC type reactor. Still, the role of the rotational speed of the working electrodes in an RDBER when operated as a MEC remains underexplored and will likely diverge from the behavior observed in conventional RBCs, given that in the RDBER the rotating anodes are fully submerged in the bulk liquid during MEC operation.

Although the RDBER was originally designed as a scale-up attempt for a thermophilic, oxic microbial electrosynthesis process, both anodic and cathodic biofilms have been successfully cultivated in the reactor in proof-of-concept studies (Hackbarth et al., 2023). However, systematic research assessing hydrogen production and evaluating the potential and limitations of this bioelectrochemical reactor operated as a MEC under controlled and defined laboratory conditions is lacking. Addressing this gap is crucial not only for gaining valuable insights that can directly inform reactor design improvements but also for providing baseline data to develop a future model as a foundation for potential scale-up efforts.

Therefore, in a series of batch experiments, we cultivated the model exoelectrogens *Shewanella oneidensis* and *Geobacter sulfurreducens* as a co-culture in the RDBER operated as a MEC at different working electrodes speeds while monitoring substrate degradation, current and gas production. These anode-reducing model microorganisms are known to form two-species biofilms that produce higher current densities in a BES compared to pure-culture biofilms of each species (Engel et al., 2019). This increased performance is likely attributed to *Shewanella oneidensis* capacity to oxidize a wide range of substrates, such as lactate, into carbon dioxide and acetate. The acetate produced serves then as the primary carbon source for *Geobacter sulfurreducens*, which then fully oxidizes the acetate into carbon dioxide. Additionally, *S. oneidensis* plays a vital role in reducing oxygen contaminations, which would otherwise hinder the acetate oxidation process by the strict anaerobe *G. sulfurreducens.* As hydrogen shuttling from the cathode into the anodic biofilm was observed during co-cultivation of these organisms in the RDBER operated as an MEC, we attempted to mitigate this electrochemical short circuit by modifying the reactor's cathode configuration. Finally, we compare key performance indicators of the modified reactor with those of other MEC reactor concepts in the scale range of 10 L and above.

Table 1
Studies involving bioelectrochemical reactors inspired by RBCs (rotating biological contactors) and their respective study objectives. Notably, all reactors listed are single-chamber BES (bioelectrochemical systems). Rpm – revolutions per minute.

Reference	Objectives	Working volume (Total reactor volume)	Function of rotating discs (surface area)	Rotational speed	Quantification of gaseous products
(Krzemieniewski and Rodziewicz, 2005)	A rotating electrobiological contactor (REBC) was presented and operated to assess the impact of an applied current on the efficiency of nitrogen compound removal from both synthetic and real wastewater.	Four stages in series à 2 L (–)	Cathode (0.6 m^2 per stage)	60 rpm	–
(He et al., 2007)	The impact of rotating a half-submerged cathode on power production in a river sediment microbial fuel cell was assessed. Rotation enhanced cathodic oxygen availability, thereby increasing the cathodic reaction rate and resulting in higher power output.	1.3 L (–)	Cathode (0.0086 m^2)	0.5 to 2 rpm	–
(He et al., 2009)	Electricity production from ammonium was investigated using a rotating-cathode microbial fuel cell. Addition of ammonium salts led to current generation, whereas sodium chloride, nitrate, or nitrite had no effect on current production.	0.75 L (1.125 L)	Cathode (0.0475 m^2)	1.1 rpm	–
(Cheng et al., 2011)	A rotatable bioelectrochemical contactor (REBC) was designed, built, and operated as a microbial electrolysis cell with polarity inversion for methane production from low-strength wastewater. Each REBC disc was subdivided into two isolated half-discs: one immersed in the liquid bulk, the other in the gas headspace. Polarity inversion promoted the formation of a mixed-species biofilm, catalyzing both anodic acetate oxidation and cathode-driven methanogenesis.	1.75 L (ca 4 L)	Regular half-rotations resulted in polarity inversions of the half discs: the anode became the cathode and vice versa. (a total of 0.095 m^2 submerged in bulk phase)	No continuous rotation Intermittent 180° rotations every 2 h	yes
(Cheng et al., 2012)	A rotatable bioelectrochemical contactor (REBC) was operated under oxic conditions as a microbial fuel cell. Each disc was subdivided into two isolated half-discs: one immersed in the liquid bulk phase, the other in the gas headspace. Regular polarity inversion was applied to prevent the formation of inhibitory pH-gradients at the electrodes. Performance was compared between REBC operation with and without electron flow.	1.75 L (ca 4 L)	Regular half-rotations resulted in polarity inversions of the half discs: the anode became the cathode and vice versa. (a total of 0.095 m^2 submerged in bulk phase)	No continuous rotation 360° inversion once every 15 min or 180° rotation every h	–
(Sayess et al., 2013)	A microbial fuel cell was 'integrated' into a rotating biological contactor and operated with synthetic wastewater for 80 days. The impact of the C/N ratio on COD (chemical oxygen demand) and nitrogen removal was investigated under conditions with and without electron flow.	Three stages in series à 1.33 L (–)	Cathode (0.041 m^2)	3 rpm	–
(Rodziewicz et al., 2020)	A rotating electrobiological contactor (REBC) was operated on synthetic wastewater resembling effluent from soilless tomato cultivation at varying hydraulic retention times. The reactor is now referred to as either a rotating electrobiological disc contactor (REBDC) or rotating electrochemical disc contactor (RECDC) if the cathodic biofilm was manually wiped off the rotating cathodes. Currents of up to 10 A m^{-2} were applied to investigate both biotic and abiotic nitrogen and phosphorus removal.	Four stages in series à 2 L (–)	Cathode (0.6 m^2 per stage)	10 rpm	–
(Hackbarth et al., 2023)	A rotating disc bioelectrochemical reactor (RDBER) was presented, demonstrating proof-of-principle cultivation of both cathodic and anodic biofilms on the rotatable working electrodes.	Ca. 9 L (10 L)	Either cathode or anode – dependent on the organism cultivated (1 m^2)	1 rpm	yes
(Knoll et al., 2023)	An RDBER, inspired by Hackbarth et al. (2023), was designed, built, and used to analyze the robustness (in terms of current) of a model biofilm formed by *Geobacter sulfurreducens* and *Shewanella oneidensis* under rapidly changing process conditions such as anode potential and shear forces. Additionally, a mathematical model was developed to predict the system's behavior in terms of current output.	10 L (12.6 L)	Anode (0.5 m^2)	0.25 to 2 rpm	–
(Juergensen et al., 2025)	This study aimed to enhance the performance of axenic *Shewanella oneidensis* cultivation in an	10 L (12.6 L)	Anode (0.5 m^2)	–	–

(*continued on next page*)

Table 1 (*continued*)

Reference	Objectives	Working volume (Total reactor volume)	Function of rotating discs (surface area)	Rotational speed	Quantification of gaseous products
This study	RDBER operated as a microbial electrolysis cell by improving genetic strain modifications and medium optimization. This study assesses the impact of the rotational speed on the performance (hydrogen production, COD degradation) of an RDBER operated as a microbial electrolysis cell under controlled laboratory conditions, using a low-complexity anodic biofilm.	Ca. 9 L (10 L)	Anode (1 m^2)	0.25 to 2 rpm	yes

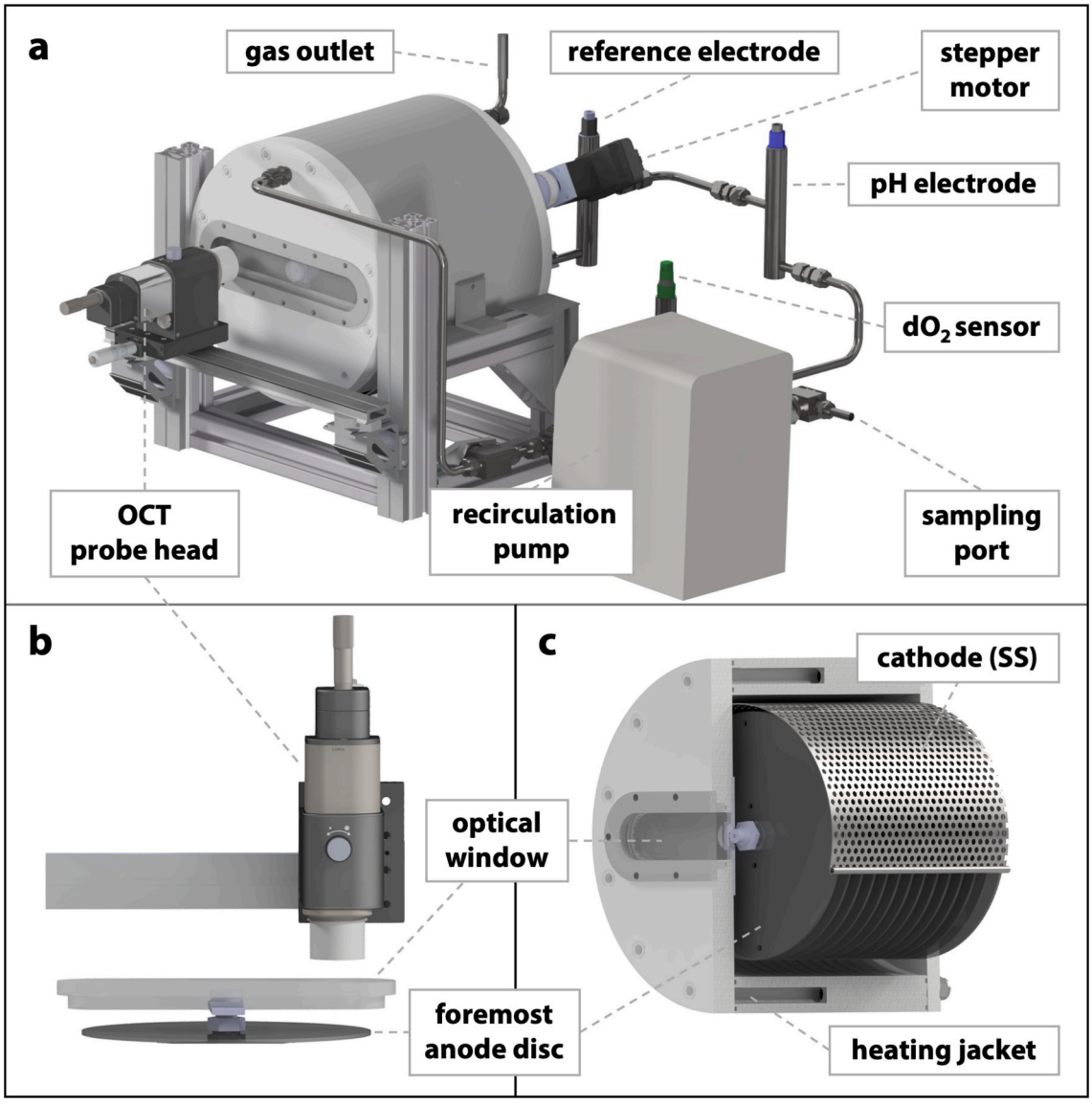

Fig. 1. Schematic 3D renderings of the RDBER used in this study. (a) Overview of the reactor and its peripheral equipment, including several measuring electrodes (pH, dO_2, reference), a recirculation pump and the OCT-probe head. (OCT – optical coherence tomography) (b) Top-down view of isolated reactor components illustrating the setup for OCT image acquisition. (c) Cross-sectional view of the reactor, depicting the anodic electrode roll and the modified counter electrode made of perforated stainless steel.

2. Material and methods

2.1. Strains and preculture conditions

Shewanella oneidensis MR-1 was routinely cultured aerobically in LB-Lennox-Medium (at 30 °C, 180 rpm), while *Geobacter sulfurreducens* PCA was pre-grown under anoxic conditions at 30 °C in BES-medium (pH 7.4). The detailed composition of this minimal medium can be found elsewhere (Hackbarth et al., 2023). Briefly, 20 mM sodium acetate and 40 mM of disodium fumarate were added as electron donor and acceptor, respectively. Mid-log phase cells were harvested and washed twice in BES-medium omitting fumarate before final inoculation of the reactor.

2.2. Reactor design

A detailed description of the design and configuration of the bio-electrochemical reactor employed for all experiments in this study has been provided in a previous publication (Hackbarth et al., 2023). The reaction chamber of this rotating disc bioelectrochemical reactor (RDBER) has an inner volume of 10 L. Relative to the working electrode area of 1 m^2 this results in a surface-to-volume ratio of 100 m^2 m^{-3}. Fig. 1 shows three 3D renderings of the reactor, providing schematic insight into its design while highlighting specific components. The working electrode assembly consists of 14 graphite discs - each with a diameter of 210 mm - mounted on a rotatable titanium shaft, which also serves as current collector. A high-resolution stepper motor on the back of the reactor (Lexium MDrive Motion Control, Schneider Electric) allows precise, load-independent control of the rotational speed of the titanium shaft. In its original configuration, the counter electrode consisted of 15 semicircular mixed metal oxide (MMO) coated titanium plates (platinode type 177, Umicore) that were mounted on four threaded titanium rods located in the lower half of the cylindrical reaction compartment (Fig. 2a shows a detailed view of a single assembled titanium plate on top of a single graphite disc anode). The individual half-disc-shaped counter electrodes were each mounted alternately between the working electrode discs with a distance of 5.5 mm to the two adjacent discs. The active counter electrode surface area of the original configuration added up to approximately 0.5 m^2.

To minimize hydrogen-shuttling in between the original titanium counter electrodes and the biofilm on the working electrode, a new counter electrode made from a bent stainless-steel (1.4571) plate was examined in this study (Fig. 1c and 2b). For this purpose, a pair of stainless-steel pipes were first screwed onto the two upper titanium rods that originally served for the mounting of the original titanium electrodes. The stainless-steel plate was bent into a round shape and welded to the stainless-steel pipes so that it was now located on top of the anodes in the upper half of the reaction chamber. A perforation in the electrode plate allows emerging hydrogen to easily escape towards the gas outlet in the upper part of the reactor and is intended to prevent evolving hydrogen bubbles from accumulating under the steel plate. The active surface area of the new stainless-steel counter electrode amounted to

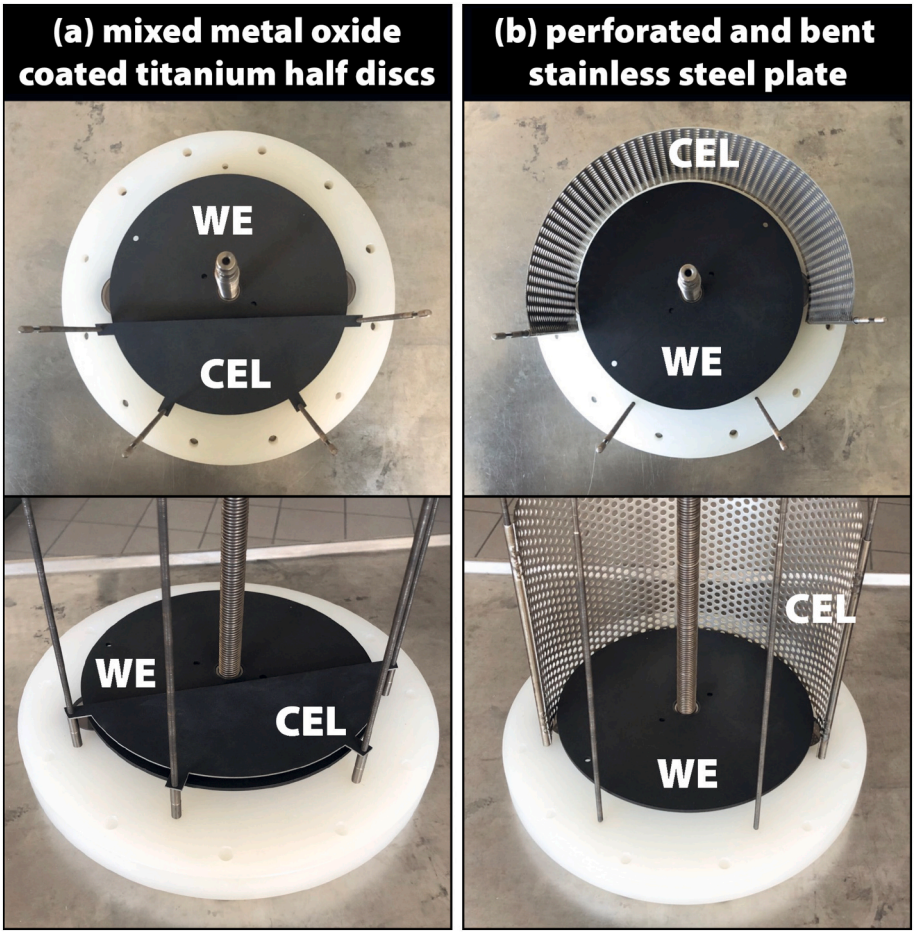

Fig. 2. Photographs of the different counter electrode (here the cathode) configurations of the RDBER used in this study. For clarity, only one of the 14 working electrode discs was installed on each picture. (a) semicircular mixed metal oxide (MMO)-coated titanium counter electrodes located in the lower half of the reactor (exemplary the photo depicts only one of the 15 counter electrodes). (b) bent and perforated stainless-steel plate (grade 1.4571) serves as modified counter electrode placed above the rotating working electrodes. WE – Working electrode; CEL – Counter electrode.

0.111 m^2.

2.3. Reactor operation

Prior to each new start-up of the reactor, the system was completely disassembled into its individual parts in order to clean them successively with isopropanol, ethanol and demineralized water. Subsequently, the reactor was reassembled and sterilized by autoclaving. The reactor was then filled with approximately 10 L of previously inoculated BES medium (pH 7.4, 20 mM sodium lactate and 20 mM sodium acetate as electron donors). This involved inoculation with *S. oneidensis* and *G. sulfurreducens* in a 9:1 ratio, resulting in an initial optical density (OD_{600}) of 0.1. Both *S. oneidensis* and *G. sulfurreducens* are well-established electroactive model organisms, extensively employed in the investigation of extracellular electron transfer (EET) mechanisms. Under anaerobic conditions, these organisms can oxidize easily degradable organic acids. The thereby released electrons are then transferred to an insoluble extracellular electron acceptor – such as metal oxides or an anode – serving as the terminal electron acceptor of an anaerobic respiration. Within our experimental setup, *S. oneidensis* carries out the partial oxidation of lactate, producing acetate and CO_2, whereas *G. sulfurreducens* utilizes acetate as an electron donor and fully oxidizes it to CO_2:

$$CH_3CH(OH)COO^- + 2H_2O \rightarrow CH_3COO^- + CO_2 + 5H^+ + 4e^-$$

$$CH_3COO^- + 2H_2O \rightarrow 2CO_2 + 8H^+ + 8e^-$$

The partial oxidation of lactate to acetate and CO_2 by *Shewanella* is coupled to the transfer of four electrons to the anode, whereas the complete oxidation of acetate to two moles of CO_2 by *G. sulfurreducens* yields in an EET of eight electrons.

A heating jacket in the reactor shell enabled a circulation thermostat-dependent control of the reactor temperature, which was kept constant at 30 °C. The medium was recirculated at a pump rate of 500 mL min^{-1}. Using a potentiostat (Interface 5000P, Gamry Instruments, Warminster, USA), a constant potential of 0 mV vs. SHE (standard hydrogen electrode) was maintained at the working electrode for each 9-day experiment while recording the current densities throughout. Once a day, the reactor's cell voltage (between the counter and working electrodes) was manually measured using a conventional multimeter. Unfortunately, this data was irretrievably lost due to a serious water spill damage. Due to the very limited amount of reliable voltage data remaining after the incident, we chose not to include calculations of the reactor's energy efficiency into this manuscript. Presenting such calculations based on insufficient data could mislead readers into interpreting these estimates as robust results. We would also like to emphasize that all other performance parameters presented in the manuscript are based on data that were not affected by the water spill. Nonetheless, interested readers are welcome to perform their own estimations based on the remaining cell voltage data, with the understanding that such calculations are subject to the limitations discussed above (See supplementary data).

The working electrodes (with a disc radius of 210 mm) were rotated at speeds of up to 2 rpm, corresponding to a tangential (tip) velocity of up to 22 mm s^{-1}. A detailed estimate of the resulting shear forces acting on the biofilm is provided by Knoll and colleagues (Knoll et al., 2023). The evolving gases (e.g. cathodic H_2 and CO_2 from the microbial oxidation of the organic acids) were collected in a gas sampling bag after passing a MilliGascounter (Ritter, Germany) for measurement of the volumetric flow rate. Analysis of the collected gases was conducted by means of a Micro Gas Chromatograph (GC) (490 Micro GC, Agilent Technologies, Germany) loaded with two carrier gases (argon and helium) and two stationary phases (CP-Molsieve 5 Å Plot and PoraPLOT U J&W GC columns, Agilent Technologies, Germany). Finally, media samples were taken twice a day in order to determine the concentration of organic acids by means of a Metrohm 881 Compact Pro Ion Exchange Chromatograph (IC) with a Metrosep Organic Acids 250/7.8 column (Metrohm, Switzerland).

All experiments were performed at least in duplicate. If not otherwise mentioned, data are presented as mean values from two independent experiments and error bars represent the absolute deviation from the mean. Given the small sample size ($n = 2$ per condition), statistical analysis was not conducted, as it would not provide meaningful inference.

2.4. Optical coherence tomography and parameters for biofilm characterization

At the end of each experiment (after 9 days), optical coherence tomography (OCT) was used for 3D visualization of the anodic biofilm, using a GANYMEDE II spectral-domain OCT system (Thorlabs GmbH, Dachau, Germany) with an LSM04 objective. The digital image processing of the OCT datasets and the calculation of the biofilm structure parameters, mean biovolume $\overline{BV}$, and mean substratum coverage $\overline{SC}$, were conducted using imageJ (Bauer et al., 2019; Schneider et al., 2012) and in-house made macros (Bauer et al., 2019) as described elsewhere (Hackbarth et al., 2023).

$\overline{BV}$ (μm^3 μm^{-2}) represents the average biovolume across all measurement positions, while $\overline{SC}$ indicates the average percentage of the anode surface covered by biofilm on a trapezoidal section of the total visualized area (marked as a green box in Fig. 5c):

BV is defined as the measured biofilm volume V_{BF} (μm^3) in relation to the visualized area A_{ST} (μm^2).

$$BV = \frac{V_{BF}}{A_{ST}}$$

As described in detail in our previous publication, A_{ST} refers to the area of a single trapezoid. The sum of all such trapezoidal areas ($\sum A_{STn}$, with n indexing each individual trapezoid) constitutes to the surface of a radial section of the visualized disc (Hackbarth et al., 2023).

Accordingly, the mean biovolume $\overline{BV}$ is calculated as the sum of all locally determined biofilm volumes divided by the surface of the radial trapezoidal area:

$$\overline{BV} = \frac{\sum V_{BFn}}{\sum A_{STn}}$$

The mean substratum coverage, $\overline{SC}$, is described as follows:

$$\overline{SC} = \frac{\sum A_{STn} - A_{uc}}{\sum A_{STn}}$$

where A_{uc} denotes the area of uncovered substratum (biofilm thickness = 0 μm.)

2.5. parameters for reactor performance characterization

COD (chemical oxygen demand) degradation rates were calculated from the IC-measured lactate and acetate degradation rates (see Section 2.3) by assuming a COD of 64 g for one mol of acetate and a COD of 96 g for one mole of lactate.

The Coulombic efficiency CE (%) of the anodic half-cell reaction was calculated as the ratio of the moles of electrons transferred to the anode (calculated from the working electrode current densities $n_{e(cd)}$), and the moles of electrons $n_{e(oa)}$ theoretically released from the full oxidation of the consumed organic acids – where the consumption is based on the collected ion chromatography data:

$$CE = 100 \times \frac{n_{e(cd)}}{n_{e(oa)}}$$

$$n_{e(cd)} = \frac{\int I(t)\, dt}{F}$$

$$n_{(oa)} = n_{acetate(consumed)} \times 8 + n_{lactate(consumed)} \times 12$$

where F is the Faraday constant and I (A) describes the measured anodic current.

The cathodic hydrogen recovery r_{cat} (%) was calculated as the ratio of the actually produced moles of hydrogen measured at the gas outlet of the reactor $n_{H_2(measured)}$, and the moles of hydrogen that theoretically could have been produced based on the measured current densities as described in $n_{H_2(cd)}$.

$$n_{H_2(measured)} = \int \frac{p \times V_{gas}(t) \times x_{H_2}(t) \times}{R \times T} dt$$

With R as the universal gas constant and $V_{gas}(t)$ being the volumetric flow rate of the total off-gas as recorded by the MiliGasCounter. $x_{H_2}(t)$ represented the volume fraction of hydrogen in the collected off-gas as measured by GC-analysis. An atmospheric pressure p of 1.013 bar and a room temperature T of 295 °C were used in the calculations.

$$r_{cat} = 100 \times \frac{n_{H_2(measured)}}{n_{H_2(cd)}}$$

$$n_{H_2(cd)} = \frac{n_{e(cd)}}{2}$$

3. Results and discussion

3.1. Impact of the rotational speed on reactors performance

As part of the iterative process of exploiting the RDBERs potential, the impact of the anodes' rotational speed on the performance of the reactor operated as a microbial electrolysis cell was assessed in a series of batch experiments. In this context, the RDBER was operated at constant anodic rotational speeds (0.25, 1 and 2 rpm) for a period of 9 days each, while recording key parameters such as current densities, hydrogen production rates, and COD removal. An axenic co-culture of *Geobacter sulfurreducens* and *Shewanella oneidensis* served as inoculum in all experiments. The working electrode potential was kept constant at 0 mV vs. SHE by means of a potentiostat. As a result, the slowest rotational speed tested (0.25 rpm) led to anodic current densities of up to 0.55 ± 0.14 A m^{-2} (corresponds to a volumetric current density of 55 ± 14 A m^{-3}). As depicted in Fig. 3, by increasing the rotational speed to 1 rpm, maximum current densities of up to 1.00 ± 0.07 A m^{-2} (100 ± 7 A m^{-3})

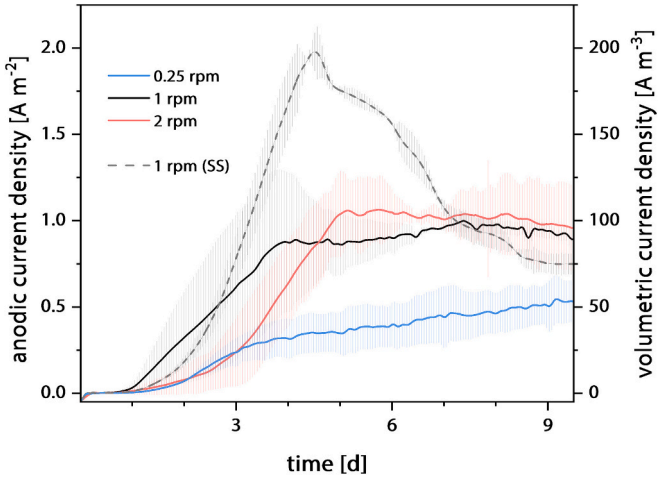

Fig. 3. Impact of the rotational speed of the working electrodes on the volumetric and anodic current densities over time (straight lines). The dotted line corresponds to the measured current densities of the modified reactor system with the new stainless-steel (SS) counter electrode at 1 rpm. Data are presented as mean values from two independent experiments ($n = 2$); error bars represent the absolute deviation from the mean.

could be achieved.

A further doubling of the speed to 2 rpm did not significantly increase the obtained current densities. Rather, a prolonged initial 'lag phase' was observed in the current density profile of the 2 rpm experiments. The COD degradation rates (see Fig. 4a and b) showed a similar correlation between rotational speed and performance. By increasing the rotational speed from 0.25 rpm to 1 rpm, COD removal approximately tripled (from 0.08 ± 0.02 to 0.25 ± 0.03 kg m^{-3} d^{-1} for the average, and from 0.13 ± 0.04 to 0.39 ± 0.04 kg m^{-3} d^{-1} for the maximum degradation rate). Operating the RDBER at 2 rpm did not result in any further significant difference in the organic acid degradation compared to the experiments conducted at 1 rpm. Another process parameter that was heavily affected by the speed of the working electrodes was the hydrogen production rate. Again, the most notable difference in both the average and maximum hydrogen production rates was evident between the 0.25 rpm and 1 rpm experiments (See Fig. 4c and d). Here, the maximum hydrogen production rate was increased by a factor of four to slightly exceed 0.4 liters of hydrogen per liter of reactor volume and day. Likewise, the average daily hydrogen production quadrupled from 0.05 ± 0.01 to 0.18 ± 0.01 L_{H_2} L_R^{-1} d^{-1}. Increasing the anodes speed to 2 rpm did not significantly change the average or maximum hydrogen production rates. Rittmann et al. employed a rotating biological contactor (non-electrified) to assess oxygen mass transfer into an aerobic biofilm growing on non-conductive discs (Rittmann et al., 1983). Yet, it is important to note that the Rittmann-RBC was operated as a gas-liquid contactor, exposing half of the disc surface to air, which may limit the comparability of their results with our study. Nevertheless, they demonstrated an increase in aeration with increasing rotational speeds up to 30 rpm. In our study, since acetate was likely not limiting, one of the primary effects of rotation during MEC operation could have been enhanced mixing and the faster removal of anodically produced protons. This effect improved as the rotational speed increased from 0.25 to 1 rpm, but no further improvement was observed beyond that speed. One possible explanation for the observed behavior in our system could be a cathode limitation resulting from the rather small surface area of the counter electrode, which may have masked further improvements in nutrient supply to the biofilm at higher rotational speeds. It should also be mentioned that no abiotic organic acid degradation or hydrogen production was measured in a sterile control experiment, nor could any influence of the rotational speed on the anodic idle current of the non-inoculated reactor be observed (see Supplementary Fig. 1).

Based on the rates described above, the respective yields of the RDBER operated as a microbial electrolysis cell were determined. Coulombic "efficiencies" (*CE*) were calculated as the ratio of electrons transferred to the anode (based on anodic current densities) and electrons released through the oxidation of the degraded organic acids (measured by means of ion chromatography). The *CE*s obtained in this manner (see Fig. 3e) ranged well above 100 % (up to 353 ± 3 % in the 0.25 rpm run). However, to be consistent with the law of conservation of energy, "efficiencies" above 100 % should be critically scrutinized and can be attributed to the fact that not all electron sources available to the anodic biofilm were included in the above calculation. Since care was taken to ensure that the employed minimal medium did not contain any respiratory electron donors accessible to the co-culture, the hypothesis was made that some cathodically produced hydrogen was re-oxidized by the anodic biofilm, resulting in an additional source of anodic electrons. Indeed, only around 60 % of the hydrogen, theoretically expected to be cathodically produced as a result of the complete anodic oxidation of the consumed organic acids (not accounting for biomass as a carbon and electron sink), was detected at the gas outlet of the reactor - with a negligible influence of the rotational speed which supports the assumption of hydrogen shuttling between the two electrodes. Although this hydrogen loss could also be caused by leaks in the reactor itself, the cathodic hydrogen recovery r_{cat}, calculated based on the moles of hydrogen that theoretically should have been produced based on the

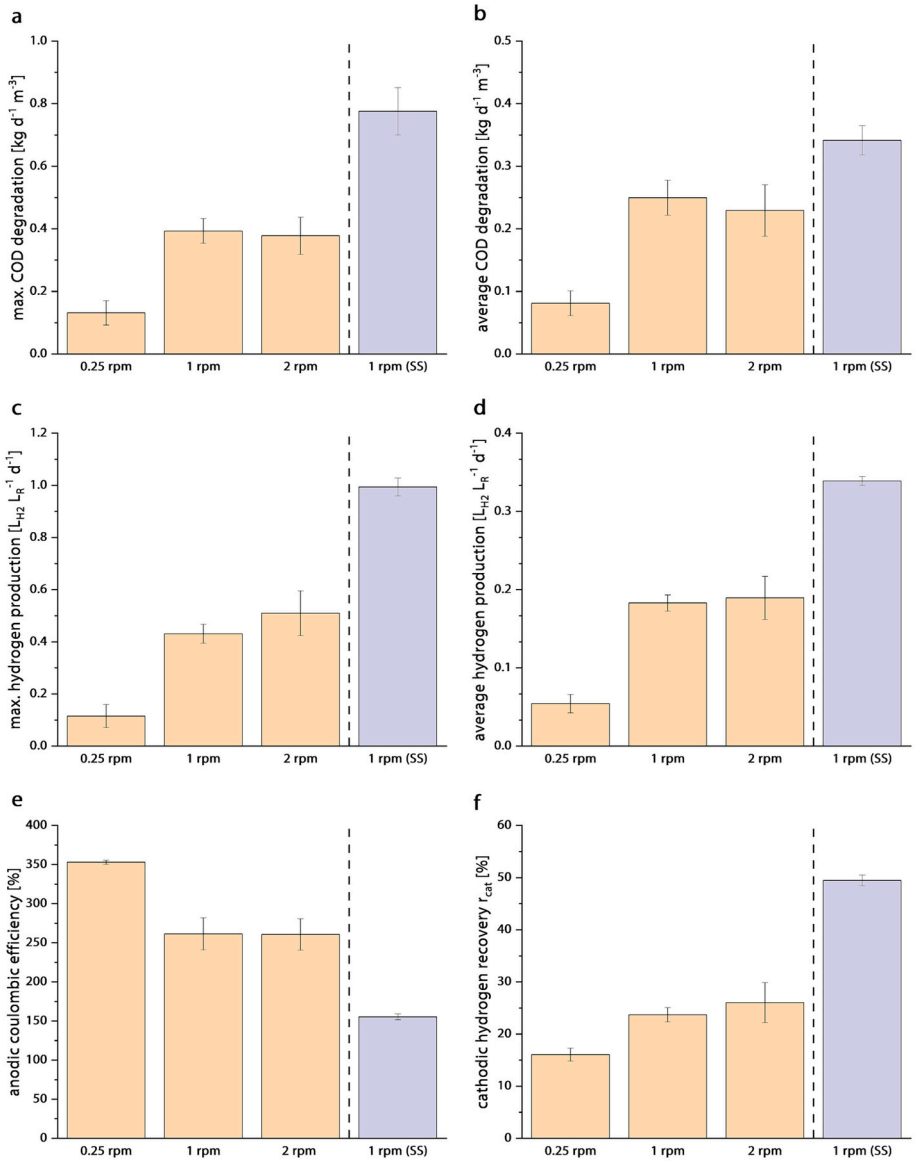

Fig. 4. Impact of the rotational speed of the anodes on different performance parameters of the RDBER operated as microbial electrolysis cell (orange). The lilac bar represents the performance of the reactor system operated with the new stainless-steel (SS) counter electrode configuration at 1 rpm. The experimental duration of all experiments shown was 9 days. (a) and (b) maximum and average COD degradation rates in kilograms COD per m^3 of reactor and day (c) and (d) maximum and average hydrogen production rates in liters (L_{H2}) per liters of reactor volume (L_R) and day. (e) coulombic "efficiencies" (CE) for the anodic half-cell reaction (ratio of the electrons transferred to the anode and the electrons theoretically released from the degraded organic acids). (f) Cathodic hydrogen recovery r_{cat}: This hydrogen yield was calculated as the ratio of the moles of hydrogen measured at the reactor's gas outlet to the theoretical moles of hydrogen produced based on the measured current densities. Data are presented as mean values from two independent experiments ($n = 2$); error bars represent the absolute deviation from the mean.

measured current densities, amounted to only around 20 %, which suggests that some of the hydrogen is re-oxidized by *G. sulfurreducens* in the anodic biofilm and thus remains trapped in a 'hydrogen loop' in the reactor. This short-circuiting of a microbial electrolytic cell, which results in a significant reduction in rates and yields of the desired electrochemical process, has previously been observed in other studies as a typical unintended side effect of a membrane-less BES (Wang et al., 2023).

Different approaches are conceivable to reduce or even prevent this phenomenon of hydrogen recycling in a microbial electrolysis cell. The apparently simplest solution is to install a semi-permeable membrane between the anode and cathode compartments. However, this is contrary to one of the main concepts of the RDBER, according to which the high ohmic losses and the complexity of the reactor, especially in the context of future scaling, are to be reduced by the elimination of the membrane. Moreover, biotic hydrogen re-oxidation might also be suppressed by the addition of specific inhibitors. For example, conjugated oligo-electrolytes were added to a membrane-less MEC, which increased hydrogen recovery by 67-fold and acetate removal by 4.4-fold as reported by Liu et al. (Liu et al., 2015). However, the regular addition of high-priced inhibitors to a biotechnological process, specifically a continuous process, would be economically unsound. Furthermore, the RDBER is designed especially for biotechnological pure culture applications due to its autoclavability and the theoretical possibility of clean-in-place. Thus, it would also be feasible to rely on other electroactive strains that are either natively (e.g. *Geobacter metallireducens, Desulfuromonas acetexigens* or *Shewanella oneidensis*) or due to genetic modifications not capable of oxidizing hydrogen. However, the limited number of electroactive microorganisms or the lack of a genetic accessibility often restricts microbial strain options. Additionally, preventing the

undesired proliferation of hydrogen oxidizing microorganisms in a mixed-species anodic biofilm presents a challenge. Therefore, we aimed for a constructive approach to minimize hydrogen recycling, as it has already been shown for other bioelectrochemical reactor concepts that a well thought-out arrangement of the electrodes and a well-managed directional flow of the fluid and gas streams in a reactor can significantly reduce electrochemical short circuits between the electrodes (Anoy et al., 2024; Giddings et al., 2015; Guo et al., 2010).

3.2. Operation of the RDBER with a modified counter electrode

In an attempt to minimize hydrogen shuttling, an alternative counter electrode configuration was developed specifically for MEC operation of the RDBER. For this purpose, the counter electrodes, which act as H_2-producing cathodes during MEC operation, were moved from the lower half of the reactor to the upper part of the reactor and thus above the rotating drum of the working electrodes. The relocation of the cathodes was intended to prevent the cathode-generated hydrogen bubbles from passing the anodic biofilm on their ascent to the gas outlet of the reactor and thus from being reoxidized by the microbes in the anodic biofilm. As part of this process, we also decided to replace the electrode material (MMO-coated titanium) with a more cost effective perforated and bent stainless steel plate (a simplified detailed photograph of both electron configurations can be seen in Fig. 2). The basic reactor structure, including the counter-electrode current collection and mounting system, has remained unchanged by these modifications and therefore either the original or the revised counter-electrode arrangement can be installed, depending on the application. To avoid any misconceptions, the authors want to clarify that, at this preliminary stage of reactor development, the modification of the counter electrode in this study was not intended to optimize the overall cell voltage or enhance the system's energy efficiency (especially since the reactor was controlled by means of a potentiostat under chronoamperometric conditions for defined laboratory conditions). Rather, the primary objective was to investigate whether bioelectrochemical short-circuiting - specifically hydrogen shuttling, which is inherent to single-chamber MECs - could be mitigated through simple and cost-effective design interventions. To this end, we employed inexpensive and widely available materials, without consideration of their electrocatalytic properties or electrochemically active surface area. The modifications were instead aimed specifically at influencing gas flow and bulk medium transport dynamics within the reactor.

We conducted batch cultivations of *G. sulfurreducens* and *S. oneidensis* in the modified RDBER under identical conditions to the previous batch experiments (e.g. 0 mV vs. SHE, 20 mM lactate, 20 mM acetate in BES-medium) to allow for direct comparison with these prior cultivations. A rotational speed of 1 rpm was selected for the working electrodes, as the previous rpm-comparison experiments indicated that increasing the speed to 2 rpm provided only marginal performance improvement – if at all –, which did not justify the increased energy consumption and wear on the reactors bearings and rotary shaft seals associated with higher rotational speeds at this point.

As illustrated in Fig. 2, the current density profile recorded in these cultivations exhibits a significantly steeper and more exponential increase, reaching a sharp peak at a twofold higher anodic current density of 1.98 ± 0.11 A m^{-2} (corresponding to a volumetric current density of 198 ± 11 A m^{-3}, compared to 100 ± 0.07 A m^{-3} for the previous cathode configuration). Following this peak, the current density declines in a wavelike manner to well below 1 A m^{-2}. This performance enhancement is similarly reflected in the specific degradation rates. The maximum COD degradation rate exceeds 0.75 kg m^{-3} reactor volume and day' compared to ~0.4 kg m^{-3} d^{-1} in the previous configuration. Likewise, the average COD removal rate raised, increasing from 0.25 ± 0.03 to 0.34 ± 0.02 kg d^{-1} m^{-2}. Notably, the increased current densities of the modified reactor also correspond to enhanced hydrogen production rates. For instance, the maximum hydrogen production rate more than doubled, rising from 0.43 ± 0.03 to 0.99 ± 0.03 L_{H_2} L_R^{-1} d^{-1}. Interestingly, while the average COD degradation rate increased by approximately 35 %, the average hydrogen production rate rose by ca. 90 %. This indicates that less hydrogen was reoxidized by the anodic biofilm and that the modification of the cathode, thus, had a positive impact on minimizing the hydrogen shuttling in the system. This effect might also be reflected in the anodic efficiency of the modified system, which is closer to 100 %, with a Coulombic efficiency (CE) of 155 ± 4 % (previously 261 ± 20 %). On the one hand, this shows that the contribution of H_2 as an additional electron donor (that was not considered when calculating the CE) could be minimized. On the other hand, it implies that at least one-third of the total electrons transferred to the anode by the anodic biofilm could still originate from hydrogen reoxidation. This estimate is based on the definition of the CE as the ratio of electrons actually transferred to the anode to the theoretical maximum derived from complete oxidation of the organic substrate. A CE of 155 % therefore implies that approximately 35 % (one third) of the electrons must originate from an additional source - most plausibly hydrogen - which was not accounted for in the theoretical calculation.

Approximately 75 % of the electrons theoretically released through organic acid oxidation were recovered in the produced hydrogen. However, this only accounts for about 50 % of the expected hydrogen yield based on the measured current densities r_{cat} (cathodic hydrogen recovery). This suggests that while the cathode modification reduced the amount of hydrogen shuttling to some extent, it could not entirely prevent it.

From an economic perspective, one of the key parameters of a MEC is the energy input required to produce a specific amount of hydrogen or to degrade a defined quantity of a given compound or COD. The electrical energy input in an MEC primarily consists of energy for pumping, heating, and the energy directly invested in the bioelectrochemical processes (Ieropoulos et al., 2024). The latter is directly dependent on the current flowing through the MEC and the applied input voltage. In this study, a potentiostat was used to maintain a constant potential of 0 mV vs. SHE on the working electrodes to ensure more consistent and comparable experimental conditions. While the current was monitored and recorded by the potentiostat, the cell voltage was manually measured during operation. Unfortunately, a significant portion of the data was lost due to water spill damage, leaving only two recorded cell voltages for the first run (single run, 0.25 rpm – old cathode) and 10 cell voltages for the final run (single run, 1 rpm – new cathode). The manually recorded cell voltages were current-dependent, ranging from 0.55 to 0.6 V in the 0.25 rpm replicate with the original reactor configuration, and from 0.78 to 1.8 V in the last replicate of the 1 rpm run with the modified stainless-steel cathode (the leftover data can be found in the supplementary material). We hypothesize that the repositioning of the counter electrode, along with the change in its material, may have negatively impacted (increased) the cell voltage due to several factors: (a) the increased distance between the counter and working electrodes; (b) the altered electrocatalytic properties of the counter electrode material; and (c) a substantial reduction in the overall surface area of the counter electrode. Since the primary objective of the modification was to reduce hydrogen shuttling rather than maximizing energy efficiency, the new counter electrode was not optimized for a minimal electrical energy input. Yet, given the limited data on cell voltage in this study, it remains unclear whether the potential benefits of this studies' counter electrode modification (e.g., higher degradation rates, increased hydrogen production, etc.) might be outweighed by a higher electrical energy demand of the modified system. While our results clearly demonstrate that bulk flow steering and deliberate electrode positioning can minimize hydrogen shuttling in a single-chamber MEC, further efforts are needed to target an optimization of the reactors energy efficiency. To reduce the cell voltage in a future reactor iteration, several modifications are conceivable, including but not limited to: (a) minimizing the distance between anode and cathode, (b) replacing stainless steel with a material that has better electrocatalytic properties,

and (c) increasing the cathode surface area, for example, by adding multiple layers of the bent perforated plates.

3.3. Optical coherence tomography of anodic biofilms

In order to obtain structural information about the anodic biofilm and especially in order to elucidate, whether or not the improvement of the reactor's performance parameters after the cathode modifications (e.g.: higher current densities) might be a consequence of a vast change in biofilm quantity or morphology, we conducted an OCT analysis of the biofilm on the foremost anode disc after each batch experiment. Since space-time-resolved in vivo monitoring of biofilm development in the RDBER was already the focus of other studies, and pausing electrode rotation to capture OCT images (which can take up to an hour) could have interfered with the experimental outcome, we conducted only an endpoint analysis of the biofilm in this study - prior to reactor disassembly and cleaning. The biofilm parameters, average biovolume ($\overline{BV}$ in μm^3 biofilm per μm^2 anode surface) and substratum coverage ($\overline{SC}$ in % of anode surface that is covered with a biofilm) were then calculated from the OCT-data sets (Wagner and Horn, 2017). Fig. 5 suggest that increasing the rotational speed from 0.25 to 1 rpm in the original reactor configuration may enhance biofilm formation, though the large error bars warrant caution in interpretation. However, the bar charts in Fig. 5 clearly show that cathode modification did not significantly increase biovolume or anode coverage, indicating that these factors do not explain the observed rise in current densities or degradation rates due to the reactor modification.

It should be mentioned that the interpretation and in particular the comparison of OCT data between different reactor systems, must generally be carried out very carefully and should not be over-interpreted. The development of biofilm morphology strongly depends on mass transfer, detachment caused by hydrodynamics and shear, as well as on growth behavior and reaction rates. The resulting morphology, in turn, affects how the flow interacts with the biofilm, influencing shear and mass transfer again. To define and distinguish the physical and biological causes and effects, much more must be known than was visualized. In this study, OCT was applied to non-moving anodes, so any biofilm movement was not documented or quantified. It is known that, in the case of streamers, (too) strong shear forces are mitigated through movement, while this flapping also increases mass transfer (Taherzadeh et al., 2012). Moreover, the OCT analysis does not reveal how cells are arranged inside the biofilm matrix. Differences in the counter electrode configuration of the two setups tested in this work resulted in different shear forces acting on the anodic biofilm and thus might have led to different biofilm densities (number of catalytically active cells per biofilm volume). In addition, a denser biofilm could lead

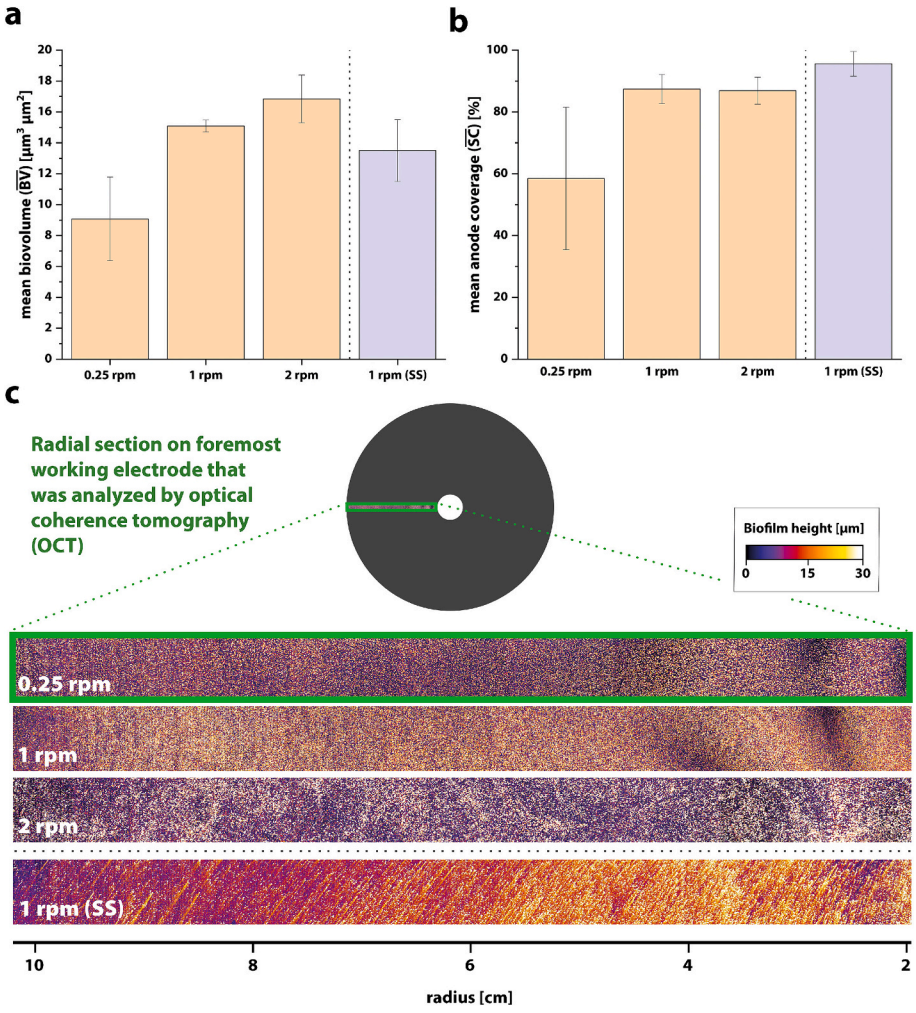

Fig. 5. OCT-derived biofilm parameters of the anodic biofilm after 9 days of operation. (a) mean biovolume and (b) mean substratum coverage. The lilac bar represents the biofilm parameters obtained from the experiments conducted with the stainless-steel (SS) counter electrode configuration. (c) representative OCT-derived height maps of a radial excerpt of the anode after 9 days of operation. The same radial section has been visualized on the working electrode in each case. Colors are coded from black (0 µm) to white (30 µm). Data are presented as mean values from two independent experiments (n = 2); error bars represent the absolute deviation from the mean.

to different diffusional behavior within the biofilm, which could impair nutrient supply.

Notably, the biofilm morphology undergoes an interesting transformation as a result of the cathode modification. In the original configuration of the RDBER, the anodic biofilms on the foremost graphite disc primarily consist of punctiform, tower-like structures. After the modification, however, distinct shooting star-like formations emerge, with tail angles that vary depending on the disc radius. Whether these are static micro-textures of the biofilm or genuine streamers cannot be deduced from the height maps. The underlying causes of this morphological change remain unclear. Potential contributing factors include: (I) reduced shear due to fewer passing hydrogen bubbles, (II) a shift in substrate utilization from hydrogen to organic acids, or (III) solely the altered hydrodynamics resulting from the displacement of the counter electrode. Due to the fact, that only 1 28th of the anode surface was characterized via OCT and that (especially in the SS cathode arrangement), the visualized first disc experiences different fluid dynamic conditions than the other electrode discs of the stack, further experiments are required to determine how homogeneously the biofilm distributes across the 14 different working electrode discs in the reactor. Thereby it should be analyzed whether growth significantly differs between discs due to suboptimal hydrodynamic conditions, caused by hydrodynamically isolated regions and in the most detrimental case, the presence of stagnant dead zones in the reactor. A hydrodynamic model, combined with an in-depth biofilm analysis using molecular biological, optical, and gravimetric methods on all electrode discs during reactor disassembly, will be essential for addressing these questions and further optimizing the system. The overall hydrodynamic design of this version of the RDBER can certainly be improved, as it was not a primary focus during the construction of this first reactor version. For instance, Introducing the recirculated substrate laterally, in addition to the front inlet, and increasing the number of perforations in the graphite discs could improve the mixing of the bulk phase in the gaps between the individual anode discs. This would enhance substrate delivery to these areas, reducing the formation of electrochemically induced pH gradients. Additionally, it would minimize the formation of a 'laminar-like' flow around the rotating electrode drum, ensuring better flow through the interelectrode space.

3.4. *Comparison of the performance of the RDBER operated as a MEC with pilot-scale MEC reactors*

For a comprehensive comparison of the RDBER's performance with other scale-up attempts, we adopted, modified, and expanded a spreadsheet from a recent literature review by Jiang et al., which systematically analyzed MEC reactor approaches and their performance (Jiang et al., 2023). As a result, Table 1 compiles construction details and performance parameters from MEC pilot studies with reactor volumes of 10 L or more. To provide a clearer visualization of the performance comparison, we plotted selected performance indicators and reactor characteristics against each other in three different scatter plots (see Fig. 6).

As shown in Table 1, the MEC reactors used in different studies vary not only in obvious parameters such as reactor volume and projected anode or cathode surface area but also in electrode materials and configurations. These differences lead to variations in electrode porosity and surface properties, which in turn influence both electrocatalytic performance and biocompatibility. Moreover, the composition of the anolyte and catholyte differs significantly across studies, ranging from nutrient- and substrate-poor, raw municipal wastewater to industrial waste streams with high organic loads, as well as synthetic, well-buffered media, such as the minimal medium used in this study. Furthermore, the reactors in these studies were operated under different temperature conditions, which can significantly impact MEC performance. Additionally, the mode of operation - whether batch, fed-batch, or continuous - along with feeding parameters such as organic loading rate and hydraulic retention time, can play a crucial role in substrate availability and, consequently, the development of the anodic biofilm.

As a result, such comparisons are inherently difficult - if not nearly impossible - to interpret quantitatively. Nevertheless, they can still offer valuable insights into the strengths and weaknesses of a reactor concept and help guide further optimization efforts. As indicated in Table 1, most published MEC scale-up attempts rely on multiple dual-chamber reactors, often arranged in a cassette-style configuration as part of a numbering-up strategy. Only 8 out of 28 pilot-scale studies with reactor volumes of 10 L or more utilize single-chamber reactors, three of which describe either the reactor examined in this study or a variation thereof. In terms of reactor volume, the 10 L RDBER presented in this study represents the lower end of pilot-scale MECs plotted in Fig. 6a, which includes reactors up to 1000 L. However, scaled up 100 L versions of the 10 L RDBER, each with a 10 m^2 working electrode surface, are currently being demonstrated and evaluated in different pilot test setups (Pott, 2023).

As shown in Fig. 5a, the maximum achieved anodic current density (~2 A m^{-2}) falls within the upper mid-range. In comparison, state-of-the-art flat-plate zero-gap reactors at the laboratory scale (with only a few milliliters of anode working volume) have achieved record current densities of up to 80 A m^{-2} - 40 times higher than the anodic current

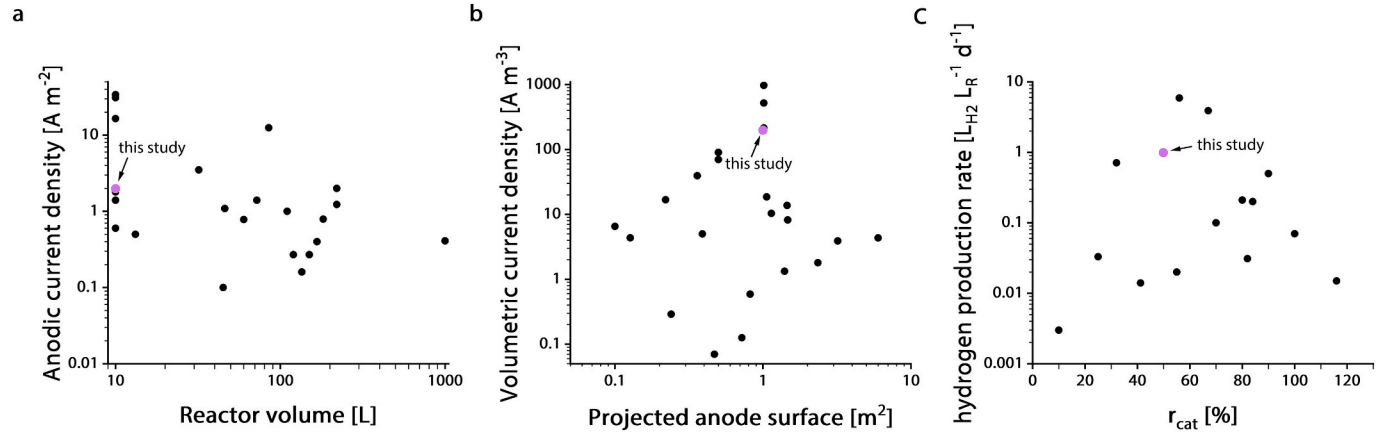

Fig. 6. Classification of performance characteristics of the RDBER (lilac dot) in comparison to pilot-scale MEC reactors (≥10 L reactor volume) from other studies (data points derived from Table 1). (a) Maximum anodic current densities reported in the literature are plotted against the respective total reactor volume. (b) Maximum volumetric current densities achieved are shown as a function of the projected anode surface. (c) Volumetric hydrogen production rates are plotted against the hydrogen yield, calculated from recorded current densities. The hydrogen yield r_{cat} corresponds to the cathodic hydrogen recovery in percent.

densities measured in this study. Yet, the RDBER's current densities are well in range with the anodic current densities obtained by Knoll and Juergensen in a very similar variation of our 10 L RDBER (1.8 A m^{-2} and 1.4 A m^{-2} respectively) (Juergensen et al., 2025; Knoll et al., 2023).

Among the upscaling attempts listed in Table 1, the reactor systems developed in the Liu lab approach for a MEC scale-up comparably high current densities of up to 34 A m^{-2}. Interestingly, all of these reactors are single-chamber MECs (Singh et al., 2021; Wang et al., 2021). In order to target anodic current densities of similar magnitude in the 10 L RDBER, several approaches are conceivable: As explained in detail in Section 3.3, a well-designed and computationally validated flow regime could play a crucial role in improving mixing in the reactor, thereby minimizing dead zones that could otherwise hinder the development of biofilms on distinct areas of some anode discs and thereby limiting the anodic current density. The rapid decline in current density in this study after reaching its peak may be due to such insufficient reactor mixing, causing localized pH drops in poorly mixed zones around some of the anode discs. This local acidification could have compromised the viability of electroactive microorganisms, potentially explaining the sudden performance loss.

The plain graphite electrodes currently used in the reactor are an unpopular choice as anode materials in pilot-scale MECs. In the original RDBER design, they were primarily selected for their highly planar surface, which facilitates precise quantitative OCT biofilm analysis. Enhancing the specific surface area of the anode could be achieved by roughening the graphite discs, utilizing alternative porous materials, for example integrating graphite felt on a support structure as working electrode discs.

Lastly, reducing the distance between the anode and cathode in the RDBER by replacing the individual rotating graphite discs, which currently serve solely as working electrodes, with sandwich electrode assemblies separated by functional spacers, could be an interesting approach: These assemblies could be arranged alternately, forming cathode and anode compartments between the discs along the rotating electrode drum. In addition to providing structural stability to the zero-gap assembly discs, the spacers could also guide the bulk flow - driven by their rotation - from the anode "compartments" into the cathode "compartments" (where the medium and gas outlets must be located), thereby preventing hydrogen shuttling.

With a projected anode surface area of 1 m^2, the 10 L RDBER falls within the mid-range of pilot-scale MECs in terms of working electrode surface (see Fig. 5b). However, when considering volumetric current densities, the RDBER ranks among the highest-performing systems (ca. 200 A m^{-3}). Only the single-chamber reactors from the Liu Lab exceed the RDBER's performance, though their volumetric current densities remain within the same order of magnitude (215–970 A m^{-3}) (Singh et al., 2021; Wang et al., 2021). This strong performance is primarily attributed to the RDBER's high surface-to-volume ratio of 100:1. Consequently, its maximum volumetric hydrogen production rate of approximately $L_{H_2}\ L_R^{-1}\ d^{-1}$ ranks among the top three reported in the literature for MEC pilots of at least 10 L reactor volume, surpassed only by the Liu Lab's systems, which could achieve 3.9 and 5.9 $L_{H_2}\ L_R^{-1}\ d^{-1}$. Interestingly, even the RDBER's average hydrogen production rate of 0.5 $L_{H_2}\ L_R^{-1}\ d^{-1}$ remains higher than most maximum hydrogen production rates reported for pilot scale MECs studies listed in Table 1. Still, the authors recognize that the controlled, axenic conditions of this study differ from real-world scenarios. In a single-chamber reactor, introducing real waste streams would promote mixed culture enrichments, possibly leading to methane formation instead of pure hydrogen production in the RDBER.

Finally, Fig. 6c shows, that the best hydrogen yield based on current density r_{cat} (cathodic hydrogen recovery) reached in this study was approximately 50 %, which is still lower compared to other reactor systems listed in Table 2. This can be explained by the prevalence of dual-chamber designs in most of the other studies, which can effectively minimize hydrogen shuttling. Notable, some of the studies in Table 1 which report exceptionally high r_{cat} values involved glucose supplementation or formation from complex organic compounds in the anolyte. Under anoxic conditions, glucose can be metabolized directly in the bulk phase, leading to additional hydrogen production that inflates yield calculations.

Table 2 shows, that high hydrogen recovery rates of dual-chamber systems - often over 80 % - seem to come with low hydrogen productivity as a key trade-off (often orders of magnitude lower than the maximum hydrogen production reported in this study). Modern dual-chamber designs, however, appear to overcome this limitation successfully. For example, Jiang et al. demonstrated a solid hydrogen production rate of 0.5 $L_{H_2}\ L_R^{-1}\ d^{-1}$, while reporting a hydrogen recovery exceeding 90 %. Yet, it is important to emphasize that dual-chamber cassette-style reactors have benefited from over a decade of optimization, whereas high-performing pilot-scale single-chamber systems like the one presented here remain relatively new and under active development. Clearly, without creative solutions to further optimize cathodic hydrogen recovery in single-chamber MECs, achieving competitiveness against well-established dual-chamber designs will be challenging. Although the reactor modifications presented in this study could only partially prevent hydrogen shuttling, we still consider carefully controlled fluid dynamics to be a promising approach for the continued optimization of single-chamber reactors.

4. Conclusions

Taken together, this study demonstrates that increasing the rotational speed of the working electrodes from 0.25 to 1 rpm improved the performance of the RDBER when operated as a microbial electrolysis cell under controlled laboratory conditions. However, further increasing the electrodes speed to 2 rpm did not result in a convincing benefit. This suggests that other, as yet unidentified, factors became limiting at higher rotational speeds. With the aim to mitigate observed hydrogen shuttling within the reactor, a modification of the counter electrode was implemented, resulting in a successful increase of the cathodic hydrogen recovery r_{cat} to 50 %. Moreover, the data indicated that the RDBER outperforms most other MEC scale-up efforts in volumetric metrics, such as hydrogen production rates ($\sim L_{H_2}\ L_R^{-1}\ d^{-1}$) and volumetric current densities (up to ~200 A m^{-3}), thanks to its favorable electrode surface-to-volume ratio of 100:1. However, without significant advancements in optimizing other critical key performance parameters - such as increasing anodic current densities (which reached only ~2 A m^{-2} in this study) and reducing the overall cell voltage between counter and working electrode - the RDBER risks being outpaced by the continued development of dual-chamber zero-gap systems utilizing a numbering-up strategy. While the scalability of these zero-gap modules is frequently framed as a straightforward engineering hurdle, it remains to be demonstrated that stackable modules can effectively process hundreds or even thousands of liters. In scenarios demanding large anodic working volumes - whether due to high wastewater throughput or a substantial presence of suspended solids - a system like the RDBER might still offer unique advantages. However, these theoretical benefits must be rigorously validated through future studies.

Abbreviations

AEM	Anion exchange membrane
BES	Bioelectrochemical system
BV	Biovolume
CE	Coulombic Efficiency
CEL	Counter Electrode
CEM	Cation exchange membrane
IC	Ion chromatography
iWW	Industrial wastewater
LB	Lysogeny broth
MEC	Microbial electrolysis cell

Table 2
Tabular summary of MEC pilot studies with ≥10 L reactor volume, reactor details and performance indicators. AEM – anion exchange membrane, CEM – cation exchange membrane, conti. – continuous, dWW – domestic wastewater, iWW – industrial wastewater, MMO – mixed metal oxide, PEM – proton exchange membrane, PBS – phosphate buffered saline, rWW – real wastewater, SHE – standard hydrogen electrode, S_{PC} – projected cathode surface, S_{PA} – projected anode surface, sWW – synthetic wastewater, WWTP – wastewater treatment plant. List adopted, modified and extended from Jiang et al., 2023 (Jiang et al., 2023).

Ref.	Total construction volume [L]	Anodic working volume [L]	Reactor type (membrane/ separator)	Anode material (projected surface [m^2])	Cathode material (projected surface [m^2])	S_{PA}/V (S_{PC}/V) [m^2 m^{-3}]	Anolyte	Catholyte	Inoculum	Operation Mode (days operated)	Anodic potential or voltage applied	Max. current density [A m^{-2}]	Max. volumetric current density [A m^{-3}]	Max H_2 production rate [L_{H2} L_R^{-1} d^{-1}]	Anodic CE [%]	r_{cat} [%]
(Baeza et al., 2017)	167	130	Multi-module dual-chamber (AEM)	Graphite fiber (3.2)	SS wire wool (1.63)	19.1 (9.76)	sWW rWW	4 g L^{-1} NaCl	MEC effluent	Batch Conti. (> 190)	1.5 V	0.4	3.9	0.031	28	82
(Brown et al., 2014)	–	60	Multi-module dual-chamber (PEM)	Graphite plate (0.39)	SS plate (0.39)	6.42 (6.42)	dWW	1 M PBS	Effluent from WWTP	Batch (>12)	0.4 mV vs. SHE	0.78	5	–	27	–
(Brown et al., 2014)	–	46	Multi-module dual-chamber (PEM)	Graphite plate (0.1)	SS mesh (16.5)	1.66 (35.87)	rWW with spiked acetate	1 M carbonate buffer	Effluent from WWTP	Conti. (>30)	0.4 mV vs. SHE	1.09	6.52	–	8	–
(Cotterill et al., 2017)	182	175	Multi-module dual-chamber (Rhinohide membrane)	Graphite felt (6.0)	SS wire wool interwoven into steel mesh (2.4)	32.9 (13.2)	dWW		rWW	Conti. (217)	0.9 V	0.79 (anode area specific)	4.34	0.003 (average)	27.7	<10
(Cotterill et al., 2018)	135	26	Multi-module dual-chamber (Rhinohide membrane)	Carbon felt (0.82)	SS wire wool (0.5)	6.0 (3.7)	dWW	0.1 M NaCl	dWW	Conti. (>180)	1.2 V	0.16 (average)	~ 0.59	0.04	–	–
(Cotterill et al., 2018)	45	–	Multi-module dual-chamber (Rhinohide membrane)	Carbon felt (1.4)	SS mesh with SS wire wool (0.6)	32 (13.33)	dWW	0.1 M NaCl	dWW	Conti. (>180)	0.9 V	0.1 (average)	~ 1.33	0.004 (average)	–	–
(Cristiani et al., 2021)	12	3.1	Tubular dual-chamber (AEM)	Graphite granules (–)	Graphite granules (–)	–	sWW		Activated sludge	Conti. (>75)	−1.3 to −2.3 V vs. SHE (cathode potential)	–	26	–	121	41 (for methane production)
(Cusick et al., 2011)	1000	910	Multi-module single-chamber (strips of glass fiber matting as separator)	Graphite fiber brush (–)	SS 304, mesh #60 (72)	- (7.2)	iWW		Wastewater and different sludges	Conti. (100)	0.9 V	0.41 (cathode specific)	7.4	0.07	–	>100 % (H_2 production from directly from sugar)
(Escapa et al., 2015)	13.2	6.6	"Single-chamber" twin units (geotextile membrane as separator)	Graphite felt (0.22)	Carbon paper with electrodeposited Ni (0.22)	16.86 (16.86)	dWW		Effluent from WWTP	Batch (~ 170)	0.7 V	~ 0.5 (anode specific)	~ 16.82	~ 0.033	120–238	10–25

(*continued on next page*)

Table 2 (*continued*)

Ref.	Total construction volume [L]	Anodic working volume [L]	Reactor type (membrane/ separator)	Anode material (projected surface [m^2])	Cathode material (projected surface [m^2])	S_{PA}/V (S_{PC}/V) [m^2 m^{-3}]	Anolyte	Catholyte	Inoculum	Operation Mode (days operated)	Anodic potential or voltage applied	Max. current density [A m^{-2}]	Max. volumetric current density [A m^{-3}]	Max H_2 production rate [L_{H2} L_R^{-1} d^{-1}]	Anodic CE [%]	r_{cat} [%]
(Gil-Carrera et al., 2013)	–	10	Twin units dual-chamber (polyester cloth)	Carbon felt (1.06)	Carbon paper with electrodeposited Ni (0.3)	106 (30.124)	dWW		homogenized anaerobic mesophilic sludge	Conti. (45)	–	~ 0.6	~ 18.63	~ 0.05	23–129	–
(Guerrero-Sodric et al., 2023)	220	135	Dual-chamber (AEM)	Carbon felt (1.47)	SS wool	6.68 (–)	sWW	5 g L^{-1} NaCl	Aerobic sludge	Conti. (>100)	0.8–1.1 V	1.23	8.21	0.1	26	70
(Guerrero-Sodric et al., 2024)	220	150	Dual-chamber cassette (AEM)	Carbon felt (1.14)	Ni-Foam (0.577)	5.18 (2.622)	iWW		Anaerobic sludge	Batch Conti. (97)	1.3 V	2	10.36	0.21	~ 20	~ 80
(Heidrich et al., 2013)	120	88	Multi-module dual-chamber (Rhinohide membrane)	Carbon felt (0.72)	SS wire wool (0.34)	6 (2.8)	dWW	50 mM PBS	Effluent from WWTP	Conti. (>90)	0.6–1.1 V	0.27	0.126	0.02	–	55
(Heidrich et al., 2014)	120	88	Multi-module dual-chamber (Rhinohide membrane)	Carbon felt (0.24)	SS wire wool (0.3)	6 (2.5)	dWW	50 mM PBS	Effluent from WWTP	Conti. (>149)	1.1 V	–	~ 0.29	0.014	–	41.2
(Huang et al., 2022)	40	38	Single-chamber (–)	Graphite felt (0.47)	Graphite felt (0.43)	11.75 (10.77)	iWW		MEC effluent	Conti. (> 60)	0.8 V	0.0	0.07	~ 0.001	1.2	–
(Isabel San-Martín et al., 2018)	–	150	Multi-module dual-chamber (AEM)	Graphite felt (2.35)	Graphite felt (2.35)	15.67 (15.67)	dWW		Activated sludge	Conti. (63)	1 V	0.27	~ 1.8	–	–	–
(Jiang et al., 2025)	85	40	Dual-chamber cassettes (CEM)	Carbon brush (–)	SS mesh (0.2)	- (2,38)	iWW	100 mM PBS	Effluent MEC	Conti. (90)	0.9 V	12.5	–	0.5	105	> 90
(Juergensen et al., 2025)	12.6	10	Single-chamber RDBER (–)	Graphite plates (0.5)	Titanium-coated half discs (0.2)	50 (20)	Buffered LB Medium enriched with 20 mM lactate.		Genetically modified *S. oneidensis*	Conti (7)	0 V vs. SHE	1.4	70	–	98.2	–
(Knoll et al., 2023)	12.6	10	Single-chamber RDBER (–)	Graphite plates (0.5)	Titanium-coated half discs (0.2)	50 (20)	Minimal medium containing 20 mM lactate		mixed culture of *S. oneidensis* and *G. sulfurreducens*	Fed-batch (47)	−0.2 to 0.2 V vs. SHE	1.8	90	–	113	–
(Leicester et al., 2020)	72	36	Multi-module dual-chamber (Rhinohide membrane)	Carbon felt (1.456)	SS mesh with SS wire wool (0.73)	20.2 (10.1)	return sludge liquor	500 mM PBS	MEC effluent	Conti. (~ 270)	0.9 V	1.4	~ 13.75	0.015	23–131	116 (hydrogen surplus not addressed in study)
(Luo et al., 2017)	21.6	19	Dual-chamber (AEM)	Carbon brush (–)	Carbon cloth coated with activated carbon	- (1.5)	sWW	3 g L^{-1} NaCl acidified to pH 4	Anaerobic sludge	Conti. (217)	0.8 V	–	0.83	0.006	–	–

(*continued on next page*)

Table 2 (*continued*)

Ref.	Total construction volume [L]	Anodic working volume [L]	Reactor type (membrane/ separator)	Anode material (projected surface [m^2])	Cathode material (projected surface [m^2])	S_{PA}/V (S_{PC}/V) [m^2 m^{-3}]	Anolyte	Catholyte	Inoculum	Operation Mode (days operated)	Anodic potential or voltage applied	Max. current density [A m^{-2}]	Max. volumetric current density [A m^{-3}]	Max H_2 production rate [L_{H2} L_R^{-1} d^{-1}]	Anodic CE [%]	r_{cat} [%]
					and platinum (0.034)											
(San-Martín et al., 2019)	32	16 L	Twin dual-chamber (CEM)	Graphite felt (0.36)	SS mesh (0.36)	11.25 (11.25)	iWW supplemented with 0.2 g L^{-1} acetate	0.1 M PBS	Digestate from WWTP	Fed-batch (103)	1 V	3.5	39.4	0.2	7–9	84
(Sim et al., 2018)	110	100	Dual-chamber (AEM/CEM)	Carbon fiber (0.127)	Carbon gas diffusion electrode (0.5)	(0.127) 4.55	sWW (acetate medium)	Tap water	MEC effluent	Batch (~ 140)	0.35–1.9 V	1.0	~ 4.36	–	–	–
(Singh et al., 2021)	10	10	Single-chamber (Cloth separator)	Carbon cloth (1.013)	Carbon cloth coated with MoP catalyst (0.17)	100 (16.89)	50 mM acetate in 100 mM PBS		MEC effluent	Batch (~ 50)	1.06 V	31.0	520	3.9	116	67
(Singh et al., 2021)	10	10	Single-chamber (Cloth separator)	Carbon cloth (1.013)	Carbon cloth coated with MoP catalyst (0.28)	100 (28.15)	50 mM acetate in 2 g L^{-1} glucose in 150 mM bicarbonate buffer		MEC effluent	Conti. (~ 85)	1 V	34.0	970	5.9	127	56
(Wang et al., 2021)	10	10	Single-chamber (Cloth separator)	Carbon cloth (1.013)	Carbon cloth (0.24)	100 (24)	iWW		Activated sludge	Conti. (~13)	1.36 V	16.5	215	0.71	–	32
(Zeppilli et al., 2020)	12	–	Dual-chamber (AEM)	Graphite granules (–)	Graphite granules (–)	–	sWW	Mineral medium	Activated sludge	Conti. (136)	2.25–4 V	–	23.5	0	24	–
This study	***10***	***~ 9***	***Single-chamber RDBER (–)***	***Plane graphite discs (1)***	***MMO-coated titanium (0.5) or type 1.4571 stainless steel (0.11)***	***100 (50 or 11.1)***	***Minimal medium containing 20 mM sodium acetate and 20 mM sodium lactate***		***Mixed culture of S. oneidensis and G. sulfurreducens***	***Batch (10)***	***0 V vs. SHE***	***1.98***	***198***	***0.99***	***155.2***	***49.9***

MET	Microbial electrochemical technology
MMO	Mixed metal oxide
OCT	Optical coherence tomography
OD	Optical density
PBS	Phosphate buffered saline
PEM	Proton exchange membrane
RBC	Rotating biological contactor
RBEC	Rotatable bioelectrochemical contactor
RDBER	Rotating disc bioelectrochemical reactor
RDE	Rotating disc electrode
REBC	Rotating electrobiological contactor
REBDC	Rotating electrobiological disc contactor
RECDC	Rotating electrochemical disc contactor
rWW	Real wastewater
SC	Substratum coverage
SHE	Standard hydrogen electrode
SS	Stainless steel
sWW	Synthetic wastewater
WE	Working electrode
WWTP	Wastewater treatment plant

CRediT authorship contribution statement

Zhizhao Xiao: Investigation, Writing – review & editing. **Max Rümenapf:** Investigation, Writing – review & editing. **Max Hackbarth:** Supervision, Methodology, Investigation, Conceptualization, Writing – original draft. **Andrea Hille-Reichel:** Conceptualization, Writing – review & editing. **Harald Horn:** Supervision, Funding acquisition, Conceptualization, Writing – review & editing. **Johannes Eberhard Reiner:** Visualization, Supervision, Methodology, Investigation, Conceptualization, Writing – review & editing, Writing – original draft.

Funding

This work was supported by a grant of the Federal Ministry of Education and Research (BMBF) as part of the BROWSE project, no. 031B1053A.

Declaration of competing interest

The authors declare that they have no known competing financial interests or personal relationships that could have appeared to influence the work reported in this paper.

Acknowledgements

Special thanks to Axel Heidt as the person responsible for the IC measurements and to Erwin Wachter, Joachim Lang and Alfred Herbst from the metal workshop of the EBI for their efforts and support.

Appendix A. Supplementary data

Supplementary data to this article can be found online at https://doi.org/10.1016/j.biteb.2025.102208.

Data availability

Data will be made available on request.

References

Anoy, M.M.I., Hill, E.A., Garcia, M.R., Kim, W.J., Beliaev, A.S., Beyenal, H., 2024. A directional electrode separator improves anodic biofilm current density in a well-mixed single-chamber bioelectrochemical system. Enzym. Microb. Technol. 180. https://doi.org/10.1016/j.enzmictec.2024.110502.

Baeza, J.A., Martínez-Miró, À., Guerrero, J., Ruiz, Y., Guisasola, A., 2017. Bioelectrochemical hydrogen production from urban wastewater on a pilot scale. J. Power Sources 356, 500–509. https://doi.org/10.1016/j.jpowsour.2017.02.087.

Bauer, A., Wagner, M., Saravia, F., Bartl, S., Hilgenfeldt, V., Horn, H., 2019. In-situ monitoring and quantification of fouling development in membrane distillation by means of optical coherence tomography. J. Membr. Sci. 577, 145–152. https://doi.org/10.1016/j.memsci.2019.02.006.

Bian, B., Yu, N., Akbari, A., Shi, L., Zhou, X., Xie, C., Saikaly, P.E., Logan, B.E., 2024. Using a non-precious metal catalyst for long-term enhancement of methane production in a zero-gap microbial electrosynthesis cell. Water Res. 259. https://doi.org/10.1016/j.watres.2024.121815.

Brown, R.K., Harnisch, F., Wirth, S., Wahlandt, H., Dockhorn, T., Dichtl, N., Schröder, U., 2014. Evaluating the effects of scaling up on the performance of bioelectrochemical systems using a technical scale microbial electrolysis cell. Bioresour. Technol. 163, 206–213. https://doi.org/10.1016/J.BIORTECH.2014.04.044.

Cheng, K.Y., Ho, G., Cord-Ruwisch, R., 2011. Novel Methanogenic Rotatable Bioelectrochemical System Operated with Polarity Inversion. Environ. Sci. Technol. 45, 796–802. https://doi.org/10.1021/es102482j.

Cheng, K.Y., Ho, G., Cord-Ruwisch, R., 2012. Energy-efficient treatment of organic wastewater streams using a rotatable bioelectrochemical contactor (RBEC). Bioresour. Technol. 126, 431–436. https://doi.org/10.1016/j.biortech.2011.12.011.

Cortez, S., Teixeira, P., Oliveira, R., Mota, M., 2008. Rotating biological contactors: a review on main factors affecting performance. Rev. Environ. Sci. Biotechnol. 7, 155–172. https://doi.org/10.1007/S11157-008-9127-X/TABLES/4.

Cotterill, S.E., Dolfing, J., Jones, C., Curtis, T.P., Heidrich, E.S., 2017. Low Temperature Domestic Wastewater Treatment in a Microbial Electrolysis Cell with 1 m^2 Anodes: Towards System Scale-up. Fuel Cells 17, 584–592. https://doi.org/10.1002/fuce.201700034.

Cotterill, S.E., Dolfing, J., Curtis, T.P., Heidrich, E.S., 2018. Community assembly in wastewater-fed pilot-scale microbial electrolysis cells. Front. Energy Res. 6, 1–12. https://doi.org/10.3389/FENRG.2018.00098.

Cristiani, L., Zeppilli, M., Villano, M., Majone, M., 2021. Role of the organic loading rate and the electrodes' potential control strategy on the performance of a micro pilot tubular microbial electrolysis cell for biogas upgrading. Chem. Eng. J. 426, 131909. https://doi.org/10.1016/j.cej.2021.131909.

Cusick, R.D., Bryan, B., Parker, D.S., Merrill, M.D., Mehanna, M., Kiely, P.D., Liu, G., Logan, B.E., 2011. Performance of a pilot-scale continuous flow microbial electrolysis cell fed winery wastewater. Appl. Microbiol. Biotechnol. 89, 2053–2063. https://doi.org/10.1007/S00253-011-3130-9.

Das, I., Ghangrekar, M.M. 2024. Pilot-scale case performance of bioelectrochemical systems, in: Microbial Electrochemical Technologies: Fundamentals and applications. Wiley, pp. 555–582. https://doi.org/10.1002/9783527839001.ch22.

Engel, C., Schattenberg, F., Dohnt, K., Schröder, U., Müller, S., Krull, R., 2019. Long-Term Behavior of Defined mixed Cultures of Geobacter sulfurreducens and Shewanella oneidensis in Bioelectrochemical Systems. Front. Bioeng. Biotechnol. 7. https://doi.org/10.3389/fbioe.2019.00060.

Enzmann, F., Stöckl, M., Zeng, A.-P., Holtmann, D., 2019. Same but different-Scale up and numbering up in electrobiotechnology and photobiotechnology. Eng. Life Sci. 19, 121–132. https://doi.org/10.1002/elsc.201800160.

Escapa, A., San-Martín, M.I., Mateos, R., Morán, A., 2015. Scaling-up of membraneless microbial electrolysis cells (MECs) for domestic wastewater treatment: Bottlenecks and limitations. Bioresour. Technol. 180, 72–78. https://doi.org/10.1016/j.biortech.2014.12.096.

Gautam, R., Nayak, J.K., Ress, N.V., Steinberger-Wilckens, R., Ghosh, U.K., 2023. Bio-hydrogen production through microbial electrolysis cell: Structural components and influencing factors. Chem. Eng. J. 455, 140535. https://doi.org/10.1016/J.CEJ.2022.140535.

Giddings, C.G.S., Nevin, K.P., Woodward, T., Lovley, D.R., Butler, C.S., 2015. Simplifying microbial electrosynthesis reactor design. Front. Microbiol. 6. https://doi.org/10.3389/FMICB.2015.00468.

Gil-Carrera, L., Escapa, A., Mehta, P., Santoyo, G., Guiot, S.R., Morán, A., Tartakovsky, B., 2013. Microbial electrolysis cell scale-up for combined wastewater treatment and hydrogen production. Bioresour. Technol. 130, 584–591. https://doi.org/10.1016/j.biortech.2012.12.062.

Guerrero-Sodric, O., Baeza, J.A., Guisasola, A., 2023. Exploring key operational factors for improving hydrogen production in a pilot-scale microbial electrolysis cell treating urban wastewater. Chem. Eng. J. 469. https://doi.org/10.1016/j.cej.2023.144001.

Guerrero-Sodric, O., Baeza, J.A., Guisasola, A., 2024. Enhancing bioelectrochemical hydrogen production from industrial wastewater using Ni-foam cathodes in a microbial electrolysis cell pilot plant. Water Res. 256, 121616. https://doi.org/10.1016/j.watres.2024.121616.

Guo, K., Tang, X., Du, Z., Li, H., 2010. Hydrogen production from acetate in a cathode-on-top single-chamber microbial electrolysis cell with a mipor cathode. Biochem. Eng. J. 51, 48–52. https://doi.org/10.1016/J.BEJ.2010.05.001.

Hackbarth, M., Gescher, J., Horn, H., Reiner, J.E., 2023. A scalable, rotating disc bioelectrochemical reactor (RDBER) suitable for the cultivation of both cathodic and anodic biofilms. Bioresour. Technol. Rep. 21, 101357. https://doi.org/10.1016/j.biteb.2023.101357.

Hassard, F., Biddle, J., Cartmell, E., Jefferson, B., Tyrrel, S., Stephenson, T., 2015. Rotating biological contactors for wastewater treatment – a review. Process. Saf. Environ. Prot. 94, 285–306. https://doi.org/10.1016/J.PSEP.2014.07.003.

He, Z., Shao, H., Angenent, L.T., 2007. Increased power production from a sediment microbial fuel cell with a rotating cathode. Biosens. Bioelectron. 22, 3252–3255. https://doi.org/10.1016/j.bios.2007.01.010.

He, Z., Kan, J., Wang, Y., Huang, Y., Mansfeld, F., Nealson, K.H., 2009. Electricity Production coupled to ammonium in a Microbial fuel Cell. Environ. Sci. Technol. 43, 3391–3397. https://doi.org/10.1021/es803492c.

Heidrich, E.S., Dolfing, J., Scott, K., Edwards, S.R., Jones, C., Curtis, T.P., 2013. Production of hydrogen from domestic wastewater in a pilot-scale microbial electrolysis cell. Appl. Microbiol. Biotechnol. 97, 6979–6989. https://doi.org/10.1007/s00253-012-4456-7.

Heidrich, E.S., Edwards, S.R., Dolfing, J., Cotterill, S.E., Curtis, T.P., 2014. Performance of a pilot scale microbial electrolysis cell fed on domestic wastewater at ambient temperatures for a 12 month period. Bioresour. Technol. 173, 87–95. https://doi.org/10.1016/j.biortech.2014.09.083.

Huang, L., Wan, H., Song, S., Liu, D., Li Puma, G., 2022. Complete removal of heavy metals with simultaneous efficient treatment of etching terminal wastewater using scaled-up microbial electrolysis cells. Chem. Eng. J. 439, 135763. https://doi.org/10.1016/j.cej.2022.135763.

Ieropoulos, I.A., Singh, A., Zertuche Moreno, D., Greenman, J., 2024. Bioelectrochemical systems and their readiness for commercialisation. Curr. Opin. Electrochem. https://doi.org/10.1016/j.coelec.2024.101540.

Isabel San-Martín, M., Mateos, R., Carracedo, B., Escapa, A., Morán, A., 2018. Pilot-scale bioelectrochemical system for simultaneous nitrogen and carbon removal in urban wastewater treatment plants. J. Biosci. Bioeng. 126, 758–763. https://doi.org/10.1016/j.jbiosc.2018.06.008.

Jiang, J., Lopez-Ruiz, J.A., Bian, Y., Sun, D., Yan, Y., Chen, X., Zhu, J., May, H.D., Ren, Z. J., 2023. Scale-up and techno-economic analysis of microbial electrolysis cells for hydrogen production from wastewater. Water Res. 241. https://doi.org/10.1016/j.watres.2023.120139.

Jiang, J., Du, L., Si, B., Kawale, H.D., Wang, Z., Summers, S., Lopez-Ruiz, J.A., Li, S., Zhang, Y., Ren, Z.J., 2025. Pilot microbial electrolysis cell closes the hydrogen loop for hydrothermal wet waste conversion to jet fuel. Water Res. 268. https://doi.org/10.1016/j.watres.2024.122644.

Jourdin, L., Burdyny, T., 2021. Microbial Electrosynthesis: where do we go from Here? Trends Biotechnol. 39, 359–369. https://doi.org/10.1016/J.TIBTECH.2020.10.014.

Juergensen, N., Weiler, J.R., Knoll, M.T., Gescher, J., Edel, M., 2025. Strategic improvement of Shewanella oneidensis for biocatalysis: Approach to media refinement and scalable application in a microbial electrochemical system. New Biotechnol. 85, 31–38. https://doi.org/10.1016/j.nbt.2024.11.006.

Kim, D., Yun, N., Du, H., Moreno Jimenez, D.A., Rossi, R., 2025. Flow field design for zero-gap microbial electrolysis cells using synthetic and real wastewater. J. Power Sources 630, 236077. https://doi.org/10.1016/J.JPOWSOUR.2024.236077.

Knoll, M.T., Jürgensen, N., Weiler, J.R., Gescher, J., 2023. Predictability and robustness of anode biofilm to changing potential in microbial electrolysis system. Bioresour Technol Rep 24. https://doi.org/10.1016/j.biteb.2023.101640.

Kracke, F., Lai, B., Yu, S., Krömer, J.O., 2018. Balancing cellular redox metabolism in microbial electrosynthesis and electro fermentation – a chance for metabolic engineering. Metab. Eng. 45, 109–120. https://doi.org/10.1016/j.ymben.2017.12.003.

Krzemieniewski, M., Rodziewicz, J., 2005. Nitrogen compounds removal in a rotating electrobiological contactor. Environ. Eng. Sci. 22.

Leicester, D.D., Amezaga, J.M., Moore, A., Heidrich, E.S., 2020. Optimising the hydraulic retention time in a pilot-scale microbial electrolysis cell to achieve high volumetric treatment rates using concentrated domestic wastewater. Molecules 25, 2945. https://doi.org/10.3390/molecules25122945.

Liu, J., Hou, H., Chen, X., Bazan, G.C., Kashima, H., Logan, B.E., 2015. Conjugated oligoelectrolyte represses hydrogen oxidation by Geobacter sulfurreducens in microbial electrolysis cells. Bioelectrochemistry 106, 379–382. https://doi.org/10.1016/J.BIOELECHEM.2015.07.001.

Luo, S., Jain, A., Aguilera, A., He, Z., 2017. Effective control of biohythane composition through operational strategies in an innovative microbial electrolysis cell. Appl. Energy 206, 879–886. https://doi.org/10.1016/j.apenergy.2017.08.241.

Pott, A., 2023. PeePower [WWW Document]. URL https://www.biooekonomie-bw.de/en/articles/pm/peepower-energy-urine (accessed 2.21.25).

Rittmann, B.E., Suozzo, R., Romero, B.R., 1983. Temperature effects on oxygen transfer to rotating biological contactors. J. Water Pollut. Control Fed. 55, 270–277.

Rodziewicz, J., Mielcarek, A., Janczukowicz, W., Bryszewski, K., 2020. Electric power consumption and current efficiency of electrochemical and electrobiological rotating disk contactors removing nutrients from wastewater generated in soil-less plant cultivation systems. Water 12, 213. https://doi.org/10.3390/w12010213.

Rossi, R., Baek, G., Logan, B.E., 2022. Vapor-Fed Cathode Microbial Electrolysis Cells with closely Spaced Electrodes Enables Greatly improved Performance. Environ. Sci. Technol. 56, 1211–1220. https://doi.org/10.1021/acs.est.1c06769.

Rossi, R., Nicolas, J., Logan, B.E., 2023. Using nickel-molybdenum cathode catalysts for efficient hydrogen gas production in microbial electrolysis cells. J. Power Sources 560. https://doi.org/10.1016/j.jpowsour.2022.232594.

Rousseau, R., Etcheverry, L., Roubaud, E., Basséguy, R., Délia, M.L., Bergel, A., 2020. Microbial electrolysis cell (MEC): Strengths, weaknesses and research needs from electrochemical engineering standpoint. Appl. Energy 257, 113938. https://doi.org/10.1016/J.APENERGY.2019.113938.

Rozendal, R.A., Hamelers, H.V.M., Euverink, G.J.W., Metz, S.J., Buisman, C.J.N., 2006. Principle and perspectives of hydrogen production through biocatalyzed electrolysis. Int. J. Hydrog. Energy 31, 1632–1640. https://doi.org/10.1016/J.IJHYDENE.2005.12.006.

San-Martín, M.I., Sotres, A., Alonso, R.M., Díaz-Marcos, J., Morán, A., Escapa, A., 2019. Assessing anodic microbial populations and membrane ageing in a pilot microbial electrolysis cell. Int. J. Hydrog. Energy 44, 17304–17315. https://doi.org/10.1016/j.ijhydene.2019.01.287.

Sayess, R.R., Saikaly, P.E., El-Fadel, M., Li, D., Semerjian, L., 2013. Reactor performance in terms of COD and nitrogen removal and bacterial community structure of a three-stage rotating bioelectrochemical contactor. Water Res. 47, 881–894. https://doi.org/10.1016/j.watres.2012.11.023.

Schneider, C.A., Rasband, W.S., Eliceiri, K.W., 2012. NIH image to ImageJ: 25 years of image analysis. Nat. Methods 9, 671–675. https://doi.org/10.1038/nmeth.2089.

Schröder, U., Harnisch, F., Angenent, L.T., 2015. Microbial electrochemistry and technology: terminology and classification. Energy Environ. Sci. 8, 513–519. https://doi.org/10.1039/C4EE03359K.

Sim, J., Reid, R., Hussain, A., An, J., Lee, H.-S., 2018. Hydrogen peroxide production in a pilot-scale microbial electrolysis cell. Biotechnol. Reports 19, e00276. https://doi.org/10.1016/j.btre.2018.e00276.

Singh, L., Miller, A.G., Wang, L., Liu, H., 2021. Scaling-up up-flow microbial electrolysis cells with a compact electrode configuration for continuous hydrogen production. Bioresour. Technol. 331, 125030. https://doi.org/10.1016/j.biortech.2021.125030.

Taherzadeh, D., Picioreanu, C., Horn, H., 2012. Mass transfer Enhancement in moving Biofilm Structures. Biophys. J. 102, 1483–1492. https://doi.org/10.1016/j.bpj.2012.02.033.

Wagner, M., Horn, H., 2017. Optical coherence tomography in biofilm research: a comprehensive review. Biotechnol. Bioeng. 114, 1386–1402. https://doi.org/10.1002/BIT.26283.

Wang, L., Long, F., Liang, D., Xiao, X., Liu, H., 2021. Hydrogen production from lignocellulosic hydrolysate in an up-scaled microbial electrolysis cell with stacked bio-electrodes. Bioresour. Technol. 320, 124314. https://doi.org/10.1016/j.biortech.2020.124314.

Wang, L., Linowski, K., Liu, H., 2023. Scalable membrane-less microbial electrolysis cell with multiple compact electrode assemblies for high performance hydrogen production. Chem. Eng. J. 454. https://doi.org/10.1016/j.cej.2022.140257.

Zeppilli, M., Cristiani, L., Dell'Armi, E., Majone, M., 2020. Bioelectromethanogenesis reaction in a tubular microbial electrolysis cell (MEC) for biogas upgrading. Renew. Energy 158, 23–31. https://doi.org/10.1016/j.renene.2020.05.122.